RESEARCH ARTICLE VOLCANICA

Driving mechanisms of subaerial and subglacial explosive episodes during the 10th century Eldgjá fissure eruption, southern Iceland

William M. Moreland*[α], Thor Thordarson[α], Bruce F. Houghton[β], Gudrun Larsen[α]
[α] Institute of Earth Sciences, University of Iceland, Askja, Sturlugata 7, 101 Reykjavík, Iceland
[β] Department of Geology and Geophysics, SOEST, University of Hawai'i at Mānoa, Honolulu, HI 96822, USA

Abstract

The 10th century Eldgjá fissure eruption is the largest in Iceland in historical time. It erupted 21.0 km^3 of magma, with 1.3 km^3 as tephra in at least 16 explosive episodes from subaerial and subglacial vents, producing magmatic and phreatomagmatic deposits respectively. Grain-size distributions for these end-members show distinct differences at comparable distances from source: the former are coarser and unimodal; the latter are finer and bimodal. These distributions appear to record different primary fragmentation histories. In contrast, the vesicle-size distributions of pyroclasts from each type of deposit show the magma was fully expanded and underwent similar vesicle nucleation and growth prior to fragmentation. This indicates that the role of glacial water was comparatively late-stage, re-fragmenting an already disrupting magma by quench granulation. The presence of microlite-rich domains within clasts reveals a history of complex conduit evolution, during the transition from a continuous dyke to focused, discrete vents.

Útdráttur

Basaltgosið á Eldgjársprungunni á 10. öld er stærsta gosið á Íslandi á sögulegum tíma. Í gosinu kom upp um 21,0 km^3 af kviku, þar af 1,3 km^3 sem gjóska í það minnsta 16 goshrinum, sem voru magmatísk gos á sprungureinum sem lágu utan Mýrdalsjökuls og freatómagmatísk gos á reinum undir jöklinum. Kornastærðardreifing gjóskunar frá þessum gosgerðum, framkvæmd á sýnum sem tekin voru í sömu fjarlægð frá upptökum, er mög frábrugðin hvor annarri: magmatíska gjóskan er grófkorna og eintoppa, en freatómagmatíksa gjóskan er fínni í korninu og tvítoppa. Þessi mismunur í kornastærðardreifingu endurspeglar mismunandi sundrunarferli kvikunnar í gosi. Aftur á móti, þá sýnir blöðrustærðardreifing, eins og hún er mæld í vikurkornum frá hvorri gjóskugerðinni um sig, að kvikan var full-blásin áður en að hún sundraðist og að blöðrumyndun og -vöxtur í báðum tilfellum var mjög svipaður. Þetta bendir til þess að þennsla kvikugasa hafði komið af stað sundrun á kvikunni áður en að hún komst í snertingu við utanaðkomandi vatn efst í eða beint ofan við gosrásina. Snertingin við utanaðkomandi vatn einfaldlega leiddi til frekari sundrunar á vikurmolunum vegna hraðkælingar. Örkristalla innlyksur í gjóskukornunum endurspegla flókna þróun á kvikunni efst í gosrásinni á þeim tíma sem virknin afmarkast við einstök gígop.

Keywords: Vesicle number density; Fissure eruption; Subglacial; Phreatomagmatic; Eldgjá

1 Introduction

Icelandic eruptions can have significant impacts on the atmosphere and hence on aviation and the global economy, as demonstrated by the 2010 eruption of Eyjafjallajökull [Gudmundsson et al. 2012; Langmann et al. 2012]. This is primarily due to the wind-advected ash plumes produced by these events. Plume height and dispersal and tephra sedimentation are strongly influenced by discharge rate and total grain size of the tephra [Mastin et al. 2009]. So, it is essential to understand all aspects of shallow conduit processes for such eruptions, and to constrain accurately eruptive volumes, particularly for the very fine ash fraction (< 125 µm) as it has the greatest potential for widespread impacts and disruption.

'Dry' or magmatic fragmentation is driven by the explosive release and expansion of magmatic volatiles [Gonnermann 2015; Mangan and Cashman 1996; Sparks 2003] and so to understand dry fragmentation it is necessary to understand processes, depths, and rates of vesiculation. When external water has access to the erupting magma during an eruption, as was the case for the subglacial eruptions of Eyjafjallajökull 2010 or

*Corresponding author: william.moreland@ingv.it
Now at: Istituto Nazionale di Geofisica e Vulcanologia - Osservatorio Etneo Piazza Roma 2, 95123 Catania, Italy

Grímsvötn 2011 [Stevenson et al. 2013], it is thought that explosive magma–water interaction (phreatomagmatism) will increase the abundance of fine ash particles present in the tephra [Kokelaar 1986; Wohletz et al. 2013; Wohletz 1986]. However recent papers have suggested that direct magma–water interaction is difficult, especially in the case of subplinian to Plinian eruptions [Aravena et al. 2018; Aravena et al. 2019; Houghton and Carey 2019]. Given the importance of fine-ash to impacts on aviation and infrastructure [Wilson et al. 2012], it is critical to assess the role and timing of external water in 'wet' tephra-producing eruptions.

The 10th century Eldgjá fissure eruption in southern Iceland (Figure 1) presents an excellent natural laboratory in which to study both magmatic vesiculation and the impact of external water for several reasons:

1. Eldgjá produced at least 16 voluminous and widespread tephra units which are preserved such that many can be mapped accurately and sampled for lab-based grain-size and vesicularity measurements with fine temporal resolution.

2. Eldgjá tephra units are the products of alternating (Figures 2 and 3) subaerial (dry) and subglacial (wet) explosive episodes [Larsen 2000].

3. The Eldgjá magma is basaltic, essentially aphyric, and has a relatively narrow compositional range (4.7–5.9 wt.% MgO and 14.6–16.7 wt.% FeO; Thordarson et al. [2001]) and so the magma was essentially uniform in terms of bulk physical properties.

These characteristics make Eldgjá an ideal case study for comparing the processes during dry versus wet explosive episodes because the complications which arise when comparing products of different eruptions and/or magmas of different composition are absent here.

This paper explores and quantifies shallow conduit and vent processes which influenced the nature of the explosive episodes of Eldgjá. This was achieved by a combination of field-based observations and measurements of individual clast density and vesicle-size distributions in subaerially- and subglacially-derived episodes of the tephra. New data presented here consist of isopach maps of individual units, grain-size distributions, density measurements, and vesicle-size distributions. The microtextures of the tephra allow the relative timing of shallow-conduit processes to be established.

2 The 939 CE Eldgjá eruption

2.1 Location and timing

The ~70 km long Eldgjá fissure is part of the Katla volcanic system in Iceland's Eastern Volcanic Zone. It extends from the Katla caldera below the Mýrdalsjökull glacier in the south-west, intermittently through the mountainous terrain north-east of the glacier to Eldgjá proper and almost to the edge of Vatnajökull glacier (Jóhannesson et al. [1990], Larsen [2000], and Miller [1989]; Figure 1). Eldgjá is the longest known erupting fissure system in historical time in Iceland. The vent structures on the subaerial fissure segments are ramparts and occasional cones of scoria and spatter. Unlike the 1783 CE Laki eruption [Thordarson 2003; Thordarson et al. 2003; Thordarson and Self 1993; Thordarson and Self 2003; Thordarson et al. 1996] there are no contemporary descriptions available of the eruption despite taking place about 60 years after Iceland was first settled. The Icelandic Book of Settlements, Landnámabók, was written about 200 years later and based on descriptions most likely passed on as oral tradition [Pálsson and Edwards 1972].

The Eldgjá tephra is stratigraphically constrained from below by the c. 870 CE Settlement Layer from the Vatnaöldur fissure of the Bárðarbunga-Veiðivötn volcanic system [Grönvold et al. 1995; Schmid et al. 2016] and from above by the 1158 CE deposit from Hekla [Janebo et al. 2016].

Initially, the Eldgjá eruption was dated via the Greenland ice core record to 934 CE [Hammer 1984; Hammer et al. 1980] or 938 CE [Zielinski et al. 1994; Zielinski et al. 1995]; more recent studies propose 939 CE as the eruption year [Baillie and McAneney 2015; Oman et al. 2006; Oppenheimer et al. 2018; Sigl et al. 2015]. The eruption lasted for at least a year [Oppenheimer et al. 2018] and may have persisted for several years [Thordarson et al. 2001; Zielinski et al. 1995].

At least 16 explosive episodes originated from either subglacial or subaerial fissure segments (Figure 3). In addition to the two large lava fields from the fissure (Figure 1), a smaller lava flow emanated from the Katla caldera creating the intercalated Kriki lava and jökulhlaup (glacial outburst flood) deposit [Larsen 2000]. The explosive activity of Eldgjá did not take place along the whole length of the fissure simultaneously; segments were active sequentially. Activity began at a subglacial fissure segment beneath Mýrdalsjökull and activity generally propagated north-east along the fissure with time. Tephra dispersal was dominantly to the south-east throughout the eruption (Figure 3).

2.2 Eldgjá tephra

Although Eldgjá was dominantly an effusive eruption, producing a minimum of 19.7 km^3 of lava [Sigurðardóttir et al. 2015], a significant volume of tephra was formed: about 1.3 km^3 (dense rock equivalent; Larsen [2000]). Eldgjá was a much larger event than the more extensively-studied 1783 Laki eruption which produced 14.7 km^3 of lava and 0.4 km^3 DRE of tephra [Thordarson and Self 1993]. The Eldgjá tephra deposit consists of two broad categories of material which, on the basis of the following physical characteristics, are

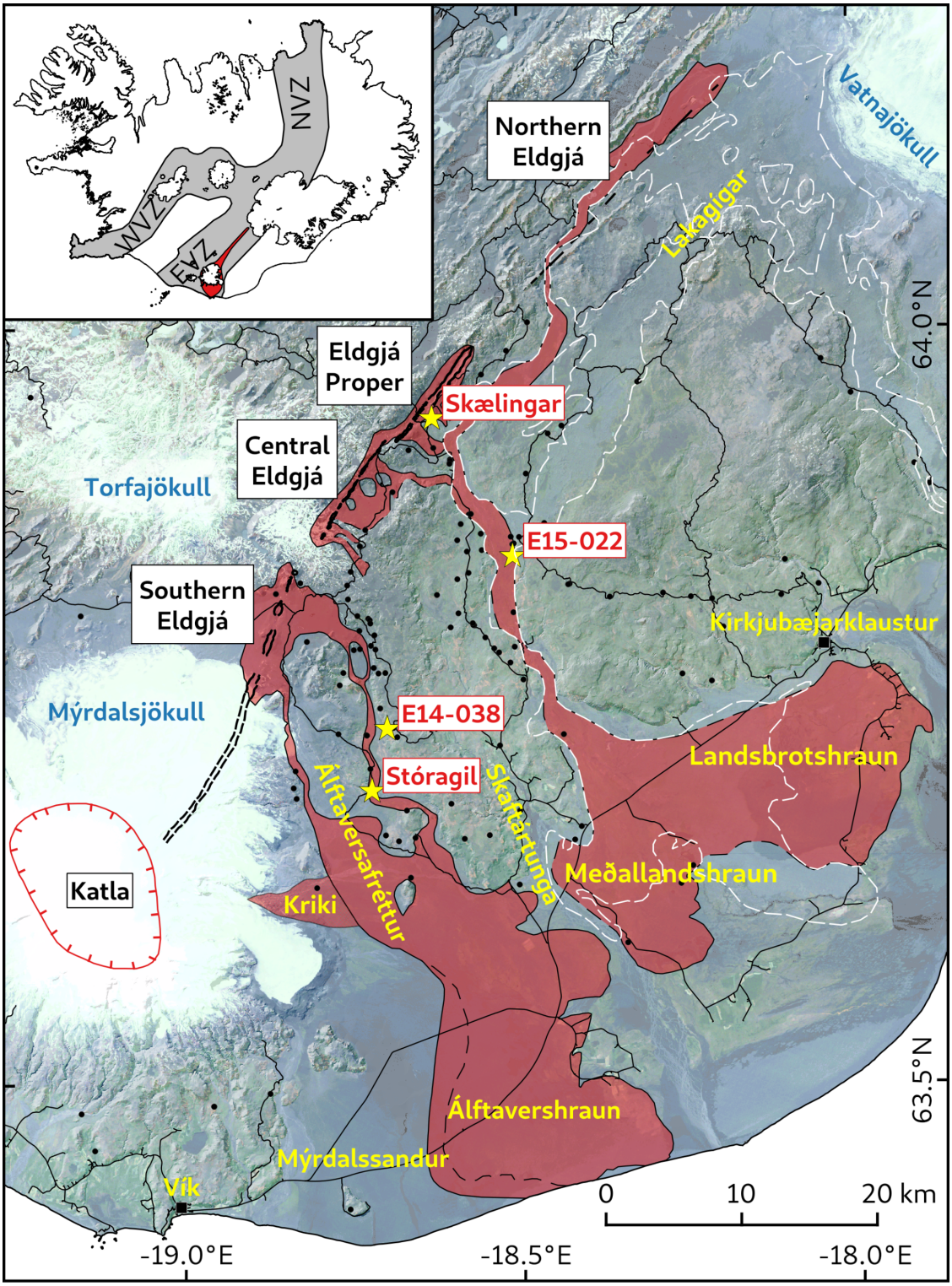

Figure 1: Map of the study area labelled with selected tephra sections (red text and stars E15-022 and E14-038 feature in Figures 2 and 6 respectively), major features of Eldgjá (black text) and various other important locations (yellow text) including the two largest settlements in the area, Vík and Kirkjubæjarklaustur (black squares). The Eldgjá fissures are outlined in thick black lines, including the subglacial portion (dashed lines), and individual segments are labelled after Larsen [2000]. The Eldgjá lava is shown in red [after Sigurðardóttir et al. 2015; Thordarson et al. 2001]. The outline of the partially-overlying 1783 CE Laki lava is shown with a dashed white line [Jóhannesson et al. 1990]. Black circles mark measured tephra sections. Roads are shown in black and the area west of the dashed line on Álftavershraun indicates the suspected lava field margin buried by deposits added to the Mýrdalssandur sand plain in historical time [Sigurðardóttir et al. 2015]. Inset is a map of Iceland showing the location of the Katla volcanic system (red) within Iceland's Eastern Volcanic Zone.

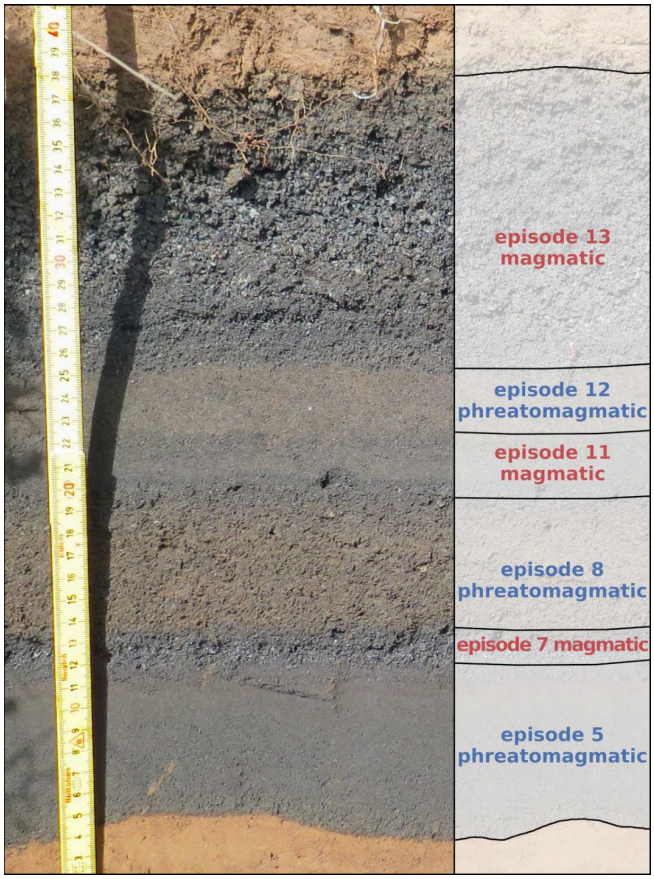

Figure 2: Typical photograph of the Eldgjá tephra deposit showing alternating magmatic and phreatomagmatic tephra fall units. Brown colouring of some phreatomagmatic units is due to presence of a significant ash fraction comprised of sideromelane glass fragments. The tephra deposit is 27 cm thick at this site, E15-022 (Figure 1), 13 km from the vent system.

termed magmatic and phreatomagmatic. On the basis of these characteristics, these two tephra types are easily distinguished in the field (Figure 2).

The magmatic tephra deposits form loose, unconsolidated layers which are rich in shiny black to blue-black achneliths typified by fluidal outer surfaces [Walker and Croasdale 1971]. The smooth, shiny surfaces of achneliths are formed by hot magmatic gases fusing the broken bubble surfaces of individual pyroclasts [e.g. Thordarson et al. 1996]. Achneliths therefore indicate when magmatic temperatures are sustained beyond primary fragmentation. The clasts are variable in shape, ranging from equant, to elongate and near-spherical, to ragged and very angular. The clast morphology does not change with grain-size with the exception that the ash-fraction contains fragments of the larger clast types, i.e. broken achneliths, vesicle walls, cuspate vesicular clasts, and more irregular and angular clasts (Figure 4A). The magmatic tephras in the medial sector of the deposit (5–25 km from vent) are generally very well to well sorted (graphic standard deviations between 0 to 2ϕ measured from 26 samples). Wall rock lithics are absent from most units but when present are red or yellow basalt and hyaloclastite fragments and form <5 modal % of the deposit. Pele's hair and tears are present in minor amounts in a few of the fall units and distinctly less abundant than in the 1783–84 Laki tephra [Thordarson and Self 1993].

The phreatomagmatic tephra deposits are brownish in colour and more structurally competent than their magmatic equivalents. The layers are rich in fine ash, and poorly sorted in the medial sector (5–25 km from vent; graphic standard deviations greater than 2ϕ measured from 30 samples). The clasts are equant and dull surfaces dominate. Scanning electron microscope images of the ash-fraction reveal their surfaces to have a coating of much finer material (Figure 4B), typical of wet explosive eruptions [e.g. Gislason et al. 2011] and thermal granulation [Colombier et al. 2019]. The ash-fraction also contains cuspate vesicular clasts like those found in the magmatic tephra but there is a greater component of irregular and blocky vesicular clasts. Besides the coating of finer material, the ash does not show features typical of phreatomagmatism such as quenching cracks, stepped features, and moss-like patterns [Büttner et al. 1999; Wohletz 1983; Zimanowski et al. 1997]. The lithic content is identical to that in the magmatic deposits.

The magmatic and phreatomagmatic units are most easily distinguished from each other by their grain-size distributions which are readily apparent in the field. Figure 5 shows the grain-size distribution of samples from two representative units, one magmatic and one phreatomagmatic, sampled at similar distances (~11 km) from their source vents. At this distance, the magmatic unit has a narrow, unimodal and positively skewed distribution with a single mode at −2ϕ. The phreatomagmatic unit has a bimodal distribution with a broad peak centred on −1.5ϕ and a tighter peak at around 5.0ϕ.

The two sections used in this study, Stóragil and Skælingar, are chosen because they represent the diversity of magmatic and phreatomagmatic tephra. The section at Stóragil is about 11 km east of the subglacial fissure segment beneath Mýrdalsjökull (Figure 1) and is over 2 m thick with nearly half being comprised of phreatomagmatic units (Figure 6). Closer to the glacier, undisturbed tephra sections are scarce due to erosion by the advance of the glacier and by jökulhlaups (floods originating from the glacier) which have occurred since the Eldgjá eruption [Larsen 2000]. The sixteen units in this section alternate between phreatomagmatic and magmatic in style, and were produced by episodes occurring at different places along fissure (Figure 3).This illustrates how activity began beneath the glacier, producing wet explosive deposits, before moving to adjacent subaerial fissure segments and becoming essentially dry. The Stóragil section is one of the most complete sections for Eldgjá, recording the largest number of individual units.

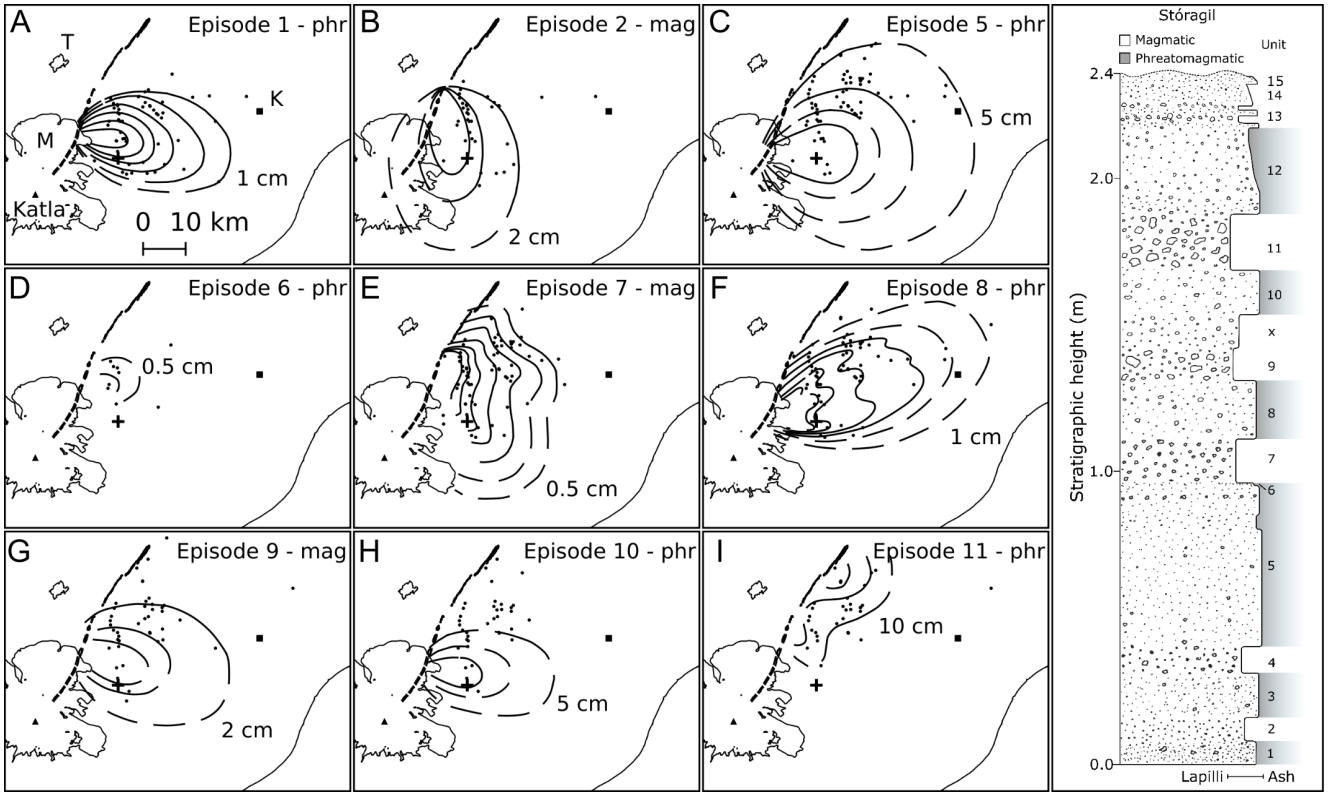

Figure 3: The sequence of explosive events as revealed by the Eldgjá tephra stratigraphy and shown using isopach maps. Note the unit labelled "x"; the unit numbers refer to Eldgjá-wide unit numbers (c.f. unit numbering on Figure 7 which refer solely to the Stóragil section). The location of the example stratigraphic section, Stóragil, is shown by a cross. The thickness of the outermost isopach is given in centimetres. The abbreviations in a) are: M, Mýrdalsjökull; K, Kirkjubæjarklaustur; T, Torfajökull. Dashed isopach lines indicate areas of inadequate data. Higher resolution isopach maps are provided in the Supplementary Material.

The section at Skælingar is less than 1 km south of the fissure at Eldgjá proper (Figure 1) and composes part of a thick tephra apron produced by the length of adjacent fissure. It is nearly 4 metres thick consisting almost entirely of magmatic tephra (Figure 6), except for the lowermost 4 cm, which contain four phreatomagmatic units. Despite being almost twice the thickness of the Stóragil section, Skælingar contains just nine units with the lowermost magmatic unit (samples 9 to 20 in Figure 6) accounting for 65 % of the tephra thickness at this site. An abrupt shift in grain-size occurs 2.5 metres from the base of the Skælingar section (units sk6 to sk9 in Figure 6) with a thin coarse ash to fine lapilli fall immediately overlying a thicker bomb layer.

The bulk of the two sections do not contain the same units; the units preserved at Stóragil are stratigraphically lower than those at Skælingar. The lowermost 4 cm of Skælingar contains phreatomagmatic units which have not been identified but which are likely present at Stóragil.

3 Methods

3.1 Fieldwork and sampling

The Eldgjá deposit was mapped by measuring individual unit thicknesses in 141 tephra sections across Iceland (Figure 1). By constructing isopach maps from the individual thickness data it was possible to reconstruct the sequence of explosive activity and the approximate sources of the tephra units (Figure 3). Unfortunately, this has not provided further constraints to the duration of the eruption.

The tephra sections at Skælingar and Stóragil were logged, individual units described in detail, and sampled for both density and grain-size analysis. The density sampling technique follows [Houghton and Wilson 1989]. Each sample consists of 100 pyroclasts between 8 and 32 millimetres in diameter (−3 to −5ϕ) collected from a horizon not more than 3 clasts thick. This size range ensures a large enough surface area in subsequent thin sections for image analysis whilst attempting to exclude any significant post-fragmentation

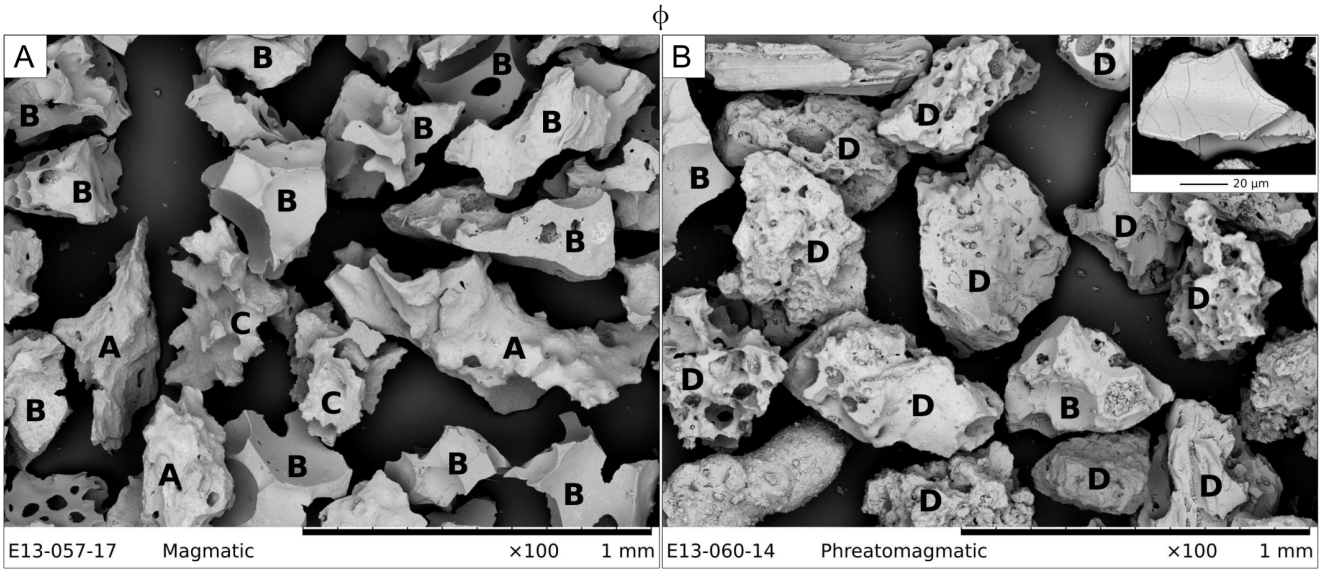

Figure 4: Scanning electron microscope images of [A] magmatic and [B] phreatomagmatic tephra (2ϕ) with clasts labelled by morphological type. The magmatic tephra is from unit 5 of Skælingar and exhibits achneliths (A), cuspate vesicular (B), and partially achnelithic (C) clasts. The phreatomagmatic tephra is from unit 3 of Stóragil and contains cuspate vesicular clasts as in the magmatic sample and irregular and blocky clasts (D). All clasts in the phreatomagmatic sample are covered in a much finer material. Inset top right is an example phreatomagmatic clast from La Fossa [Büttner et al. 1999] showing quenching cracks typical of molten fuel–coolant interaction; note the lack of any quenching cracks in the Eldgjá phreatomagmatic sample.

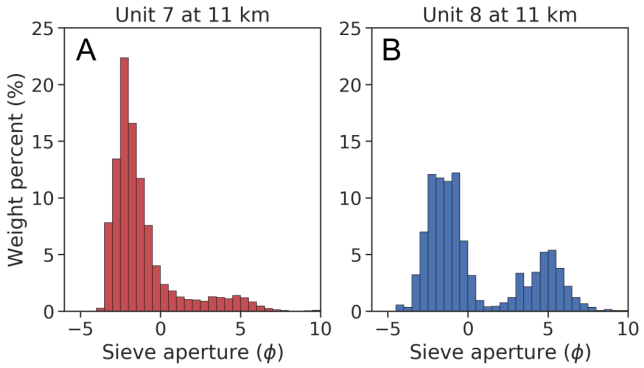

Figure 5: Representative grain-size distributions of Eldgjá tephra, each sampled from ~11 km from their respective source vents: [A] magmatic tephra from unit 7 at E14-038 (Figure 1); [B] phreatomagmatic tephra from unit 8 at Stóragil (Figure 1).

expansion of vesicles. The small sampling interval is used to justify the assumption that the clasts in each sample represent magma ejected from the vent during very narrow time windows.

The samples were numbered as follows, using E13-057-09-100 as an example: E, for Eldgjá; 13 for the year the sample was collected in (2013); 057 refers to the tephra section location number (57th site that year); 09 refers to the sample bag number (9th bag from that site, e.g. sample numbers in Figure 6); and in the case of density samples the final number (100 in this example) refers to the number of the individual clast (e.g. Figure 7).

3.2 Density and bulk vesicularity

The samples were first cleaned in a sonic bath to remove any fine particles, and then dried in an oven overnight at 40 °C. The pyroclasts were weighed, wrapped in Parafilm M to waterproof them, and weighed again, this time suspended in deionised water by a wire cage. The density of the pyroclast was then calculated using Archimedes' principle. Density was converted to vesicularity using a melt density of 2900 kg m^{-3} which was calculated from an average Eldgjá tephra whole-rock major element composition (Table 1) using the method of Bottinga and Weill [1970]. The whole-rock compositions were measured using a Spectro Ciros inductively-coupled plasma optical emission spectrograph at the University of Iceland. The density calculation also requires an estimation of temperature and water content which were calculated using the methods of Neave and Putirka [2017] and Waters and Lange [2015] respectively; the values used were 1080 °C and 1 wt.%.

3.3 Textural analysis

Polished thin sections were made from pyroclasts selected from the central (mean ± 0.5 × standard deviation) portion of representative density distributions.

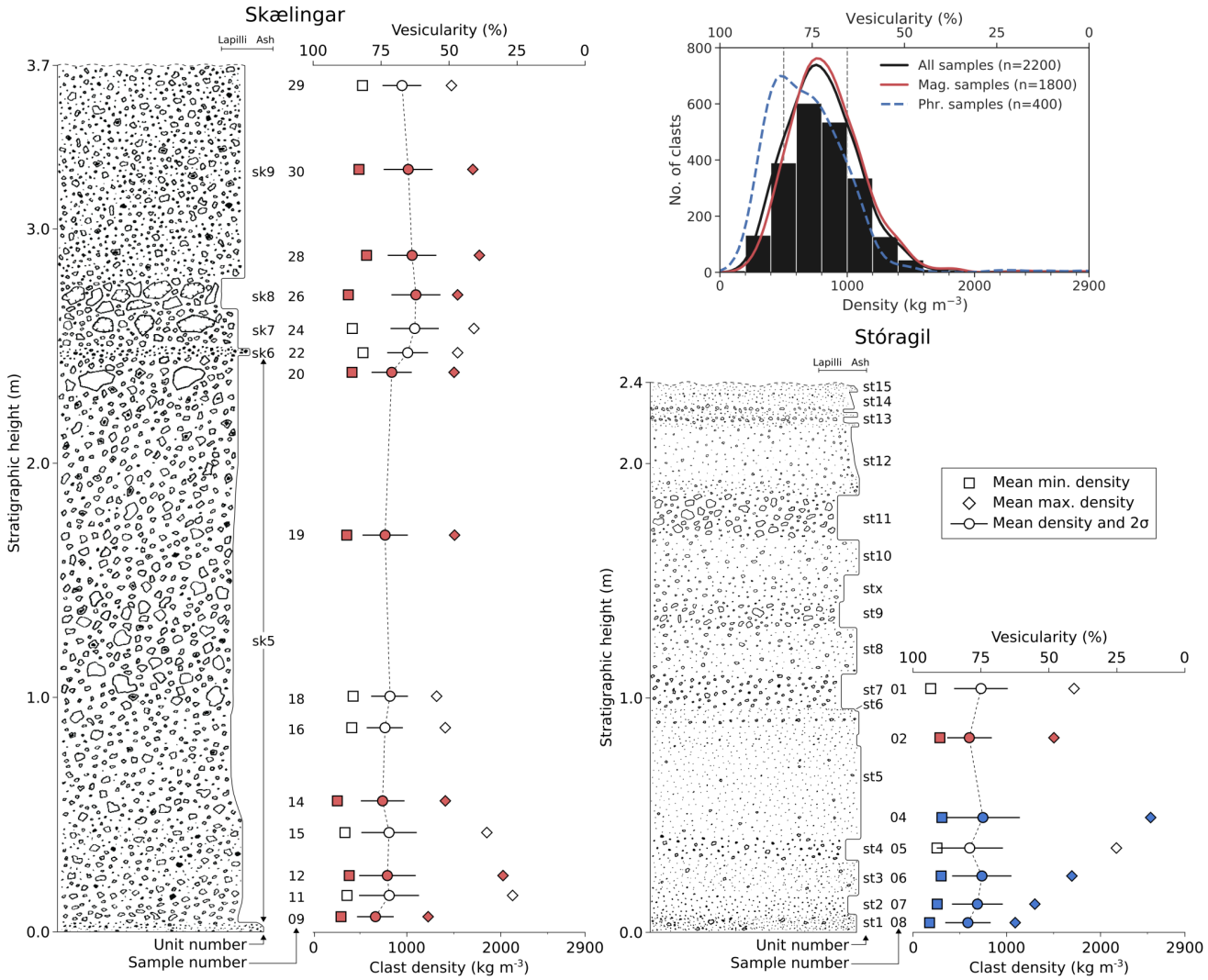

Figure 6: Stratigraphic logs of Skælingar and Stóragil with results of density analysis. Where symbols are coloured (red for magmatic, blue for phreatomagmatic) those samples have also undergone vesicle-size analysis (see Table 2). All uncoloured symbols are from magmatic units. The minimum and maximum densities for each sample were calculated from the mean of the lowest and highest three pyroclasts in each sample respectively. Inset is a histogram of all 2200 clast density measurements with kernel density estimate curves for magmatic and phreatomagmatic clasts.

Nested sets of images of the thin sections were acquired over four magnifications following Shea et al. [2010]. The first level of magnification (~4.5×) was collected on a desktop scanner. Backscattered electron images at 50×, 100×, and 250× magnification were collected on a Hitachi TM3000 scanning electron microscope at the University of Iceland. The images were processed and made binary in the free and open-source raster graphics editor GNU Image Manipulation Program. During processing, broken bubble walls were redrawn to best represent the state of the foam immediately prior to fragmentation. The binary images were analysed using the free and open-source image processing software ImageJ [Schneider et al. 2012]. Each vesicle in the reference area was counted and measured for area.

Data processing was carried out using a python script [Moreland 2019] following the general method laid out by Shea et al. [2010]. ImageJ results for each magnification level were collated to give the total bubble count and the reference area in each image. The area of each vesicle was then converted to a diameter of an equivalent circle. A minimum vesicle size was imposed based on the error associated with measuring circular objects represented by square pixels, here an 11 × 11 pixel limit was set corresponding to an equivalent diameter of 7 µm at the 250× magnification level. As the vesicle sizes cover several orders of magnitude, geometric binning was used rather than linear (equivalent diameter multiplied by $10^{0.1}$). The number of vesicles per unit area, N_A, was calculated for each bin in each magnification level. Using the minimized ΔN_A method of Shea et al. [2010], data from each magnification was

merged, ensuring as smooth a transition as possible. The method of Sahagian and Proussevitch [1998] was used to convert from number of vesicles per unit area, N_A, to number per unit volume, N_V. This method relies upon the assumption that the vesicles are spherical which is generally true in these samples. The number per unit volume does not account for the volume that the bubbles themselves take up and so a correction must be applied by dividing N_V by 100 – bulk clast vesicularity [Shea et al. 2010]. This gives the number of vesicles per unit volume of melt alone, $N_V{}^m$ (Table 2).

The results of the vesicle-size analyses are presented as vesicle volume distributions (histograms showing the volume fraction contributed by each vesicle size bin) and cumulative vesicle volume distributions. In order to quantify the similarity of the vesicle volume distributions, a two-sample Kolmogorov–Smirnov test was used. This is a nonparametric test of the equality of two distributions which in this case is the cumulative vesicle volume distribution of each sample tested against every other sample in turn. The resulting p-value gives an indication of how similar the distributions are; if it is below 0.1 then the distributions can be considered statistically different. This calculation was carried out using the `ks_2samp` function from the Python `SciPy` package [Jones et al. 2001].

3.4 Component-analysis

The external morphology of Eldgjá tephra shows little variability within each sample and so standard component analysis was omitted. However, once thin sections were made for the vesicle-size analysis it became clear that the clasts were composed of contrasting domains of glass with varying quantities of microlites. For this reason, the thin sections were qualitatively classified by their microlite content into one of three classes: microlite-poor, if the thin section was dominantly free of microlites (glass appears golden; Figure 8); microlite-rich, if it was dominated by microlites (glass appears black; Figure 8); and mixed, if it contained domains of both textures.

Table 1 – Average Eldgjá tephra major element composition used in melt density calculation

$n = 21$	wt.%	1σ
SiO_2	47.64	0.67
TiO_2	4.56	0.10
Al_2O_3	12.91	0.25
FeO^*	14.86	0.27
MnO	0.22	0.01
MgO	5.24	0.25
CaO	10.15	0.46
Na_2O	2.96	0.11
K_2O	0.75	0.07

3.5 Grain-size analysis

Bulk tephra samples were manually sieved at 0.5ϕ intervals down to 4ϕ. Material between 3 and 10ϕ was analysed on a SediGraph 5120 X-ray particle analyzer at the University of Iceland which measures the gravity-induced settling rates of different size particles in a liquid of known density. The two sets of data were then manually spliced.

4 Results

4.1 Clast density and bulk vesicularity

The mean density of the 2200 clasts collected for this study (22 samples with 100 clasts each) is $820 \pm 310\,kg\,m^{-3}$ (1σ; equivalent to a vesicularity of 71 ± 11 %; Figures 6 and 7, Table 2). Of the 22 samples, 18 are from magmatic units; the mean density of these 1800 clasts is $840 \pm 300\,kg\,m^{-3}$ (70 ± 10%). The remaining 4 samples are identified as phreatomagmatic; these 400 clasts have a mean density of $690 \pm 320\,kg\,m^{-3}$ (76 ± 11 %).

4.1.1 *Skælingar*

After a sudden decrease in vesicularity from 77 % at the beginning, unit 5 has a constant vesicularity of around 73 % (Figures 6 and 7). There is a significant decrease in mean vesicularity to 65 % in unit 6, which is a coarse ash to fine lapilli unit, followed immediately by two units, 7 and 8, containing many dense bombs. The topmost unit, 9, is typified by equally low mean vesicularity plus lower maximum and minimum values (Figure 7). Kernel density estimates (Figure 7) illustrate that the magmatic density measurements are generally unimodal, Gaussian distributions; any skewness tends to be positive.

4.1.2 *Stóragil*

The phreatomagmatic units show both the narrowest and widest ranges in vesicularity found in the Eldgjá tephra (after discarding outliers; E13-060-02, 65–91%; E13-060-07, 48–92%; Figures 6 and 7). The phreatomagmatic density measurements have either broad plateau or right-skewed unimodal distributions in the kernel density estimate plots (Figure 7) with one sample (E13-060-08) appearing to be weakly bimodal. The magmatic units present in Stóragil are similar to those found in Skælingar insofar as they have lower standard deviations and higher kurtoses than the phreatomagmatic tephra (Figure 7, inset). However, two of the three magmatic units do have higher modal vesicularities than any at Skælingar.

Table 2 – Summary of vesicle-size analysis results.

Sample*	Location	Type†	Microlite texture	Density (10^3 kg m^{-3})	Vesic. (%)‡	V_g/V_l§	N_A (mm^{-2})‖	N_V (mm^{-3})¶	N_V^m (mm^{-3})**
09-100	Skælingar	mag	poor	0.72	74.6	2.94	6.14×10^1	3.09×10^3	1.22×10^4
12-095	Skælingar	mag	poor	0.76	73.3	2.75	1.32×10^2	7.48×10^3	2.80×10^4
14-098	Skælingar	mag	poor	0.91	68.0	2.13	1.64×10^2	1.05×10^4	3.28×10^4
19-100	Skælingar	mag	mix	0.69	75.9	3.15	1.53×10^2	8.98×10^3	3.73×10^4
20-099	Skælingar	mag	rich	0.90	68.3	2.15	1.32×10^2	1.05×10^4	3.30×10^4
26-097	Skælingar	mag	mix	1.21	57.6	1.36	9.96×10^1	4.80×10^3	1.13×10^4
28-099	Skælingar	mag	mix	1.12	60.6	1.54	1.34×10^2	8.72×10^3	2.21×10^4
30-097	Skælingar	mag	mix	1.00	64.9	1.85	8.62×10^1	5.87×10^3	1.67×10^4
02-092	Stóragil	mag	mix	0.56	80.3	4.08	2.55×10^2	1.11×10^4	5.63×10^4
04-100	Stóragil	phr	rich	0.56	80.4	4.10	3.88×10^2	2.34×10^4	1.19×10^5
06-097	Stóragil	phr	rich	0.89	68.9	2.22	1.46×10^2	9.27×10^3	2.98×10^4
07-097	Stóragil	phr	rich	0.71	75.1	3.02	2.77×10^2	1.72×10^4	6.90×10^4
08-099	Stóragil	phr	poor	0.58	79.7	3.93	1.16×10^2	4.45×10^3	2.19×10^4

*Sample numbers for Skælingar prefixed with E13-057 and Stóragil by E13-060
†Tephra type based on field observations, magmatic or phreatomagmatic
‡Vesicularity calculated from density using a melt density of 2850 kg m^{-3}
§Vesicle-to-melt ratio [Gardner et al. 1996]
‖N_A is number of vesicles per unit area, excluding phenocrysts
¶N_V is number of vesicles per unit of volume and is calculated from N_A using the method of Sahagian and Proussevitch [1998]
**N_V^m is N_V adjusted for vesicle volume and is calculated by (N_V × 100) / (100 – vesicularity) [Shea et al. 2010]

4.2 Microtextural observations

4.2.1 *Microlite domains*

Thin sections of both magmatic and phreatomagmatic pyroclasts reveal that many feature two distinct types of textural domains; one characterised by golden-coloured sideromelane and the other by black tachylite (Figure 8). The colouring derives from the microlite content of each domain with the sideromelane being microlite-poor (~3 % microlites by area excluding vesicles) and the tachylite being microlite-rich (30–50 %). Therefore, the terms microlite-poor (MPD) and microlite-rich domains (MRD) will be used hereafter [after Cimarelli et al. 2010].

The MRDs contain plagioclase, Fe-Ti oxides, and pyroxene in order of decreasing relative abundance and size, with plagioclase dominant. The plagioclase microlites found in the MRDs form two size populations (average lath lengths 6 µm and 20 µm); the larger is less abundant and is also found in similar abundances in the MPDs (e.g. Figure 9I). Within the MRDs, microlites commonly align with the edge of vesicles (Figure 10). Phenocrysts are very rare in both domains but when present are either plagioclase or clinopyroxene (Figure 9A).

The two domains occur in varying proportions in each thin section but each domain type is present in both magmatic and phreatomagmatic clasts (Figure 8). MRDs sometimes occur as inclusions within an otherwise MPD clast (termed mixed clasts), but not vice-versa. The MRDs vary in size from 1 mm in diameter to consisting of the entire lapilli. The contact between domains in the mixed clasts (Table 2; Figure 10) is sharp, very convoluted, and fluidal in form with complex embayments and enclaves.

Internal componentry was carried out on 117 thin sections, 81 of which were of magmatic tephra clasts and 36 of phreatomagmatic (Table 3). Of the 117 samples, 39 % were microlite-poor, 28 % were microlite-rich, and 33 % contained both domain types. The magmatic samples were 40 %, 25 %, and 36 % microlite-poor, -rich, and mixed respectively whilst the phreatomagmatic samples were 39 %, 36 %, and 25 %. There is no correlation between microlite content and clast density; microlite-rich or mixed clasts span the full range of densities (Figure 11). At Skælingar, where the majority of tephra was erupted from a single fissure segment, there is an increase in microlite-rich and mixed clasts with stratigraphic height. At Stóragil, where the units were erupted from a variety of fissure segments, there is no correlation of microlite content with stratigraphic height.

Table 3 – Summary of thin section componentry on basis of qualitative microlite content

	n	Poor (%)	Rich (%)	Mixed (%)
All thin sections	117	39	28	33
Magmatic	81	40	25	36
Phreatomagmatic	36	39	36	25

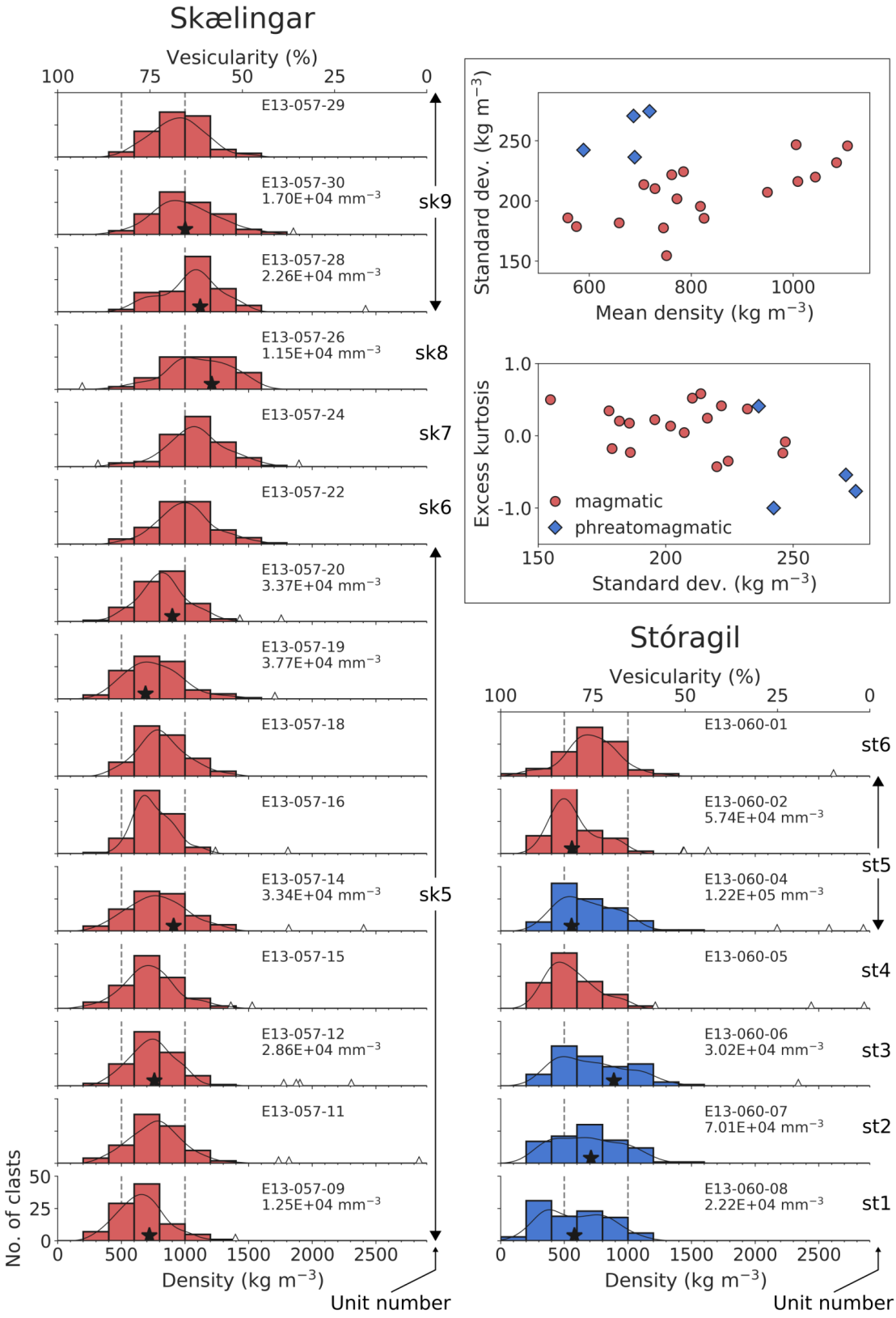

Figure 7: Density distributions of the Eldgjá tephra samples with summary statistics [inset]. Red histograms: magmatic samples; blue histograms: phreatomagmatic samples. The black curves are kernel density estimates for the density measurements. Black stars indicate the density of the pyroclasts which were used for vesicle size analysis and triangles along x-axis indicate outliers which were excluded from the statistical analyses. The vesicle number density of analysed clasts is included below the sample numbers. Vertical dashed lines at 500 and 1000 kg m^{-3} are to facilitate comparisons between samples.

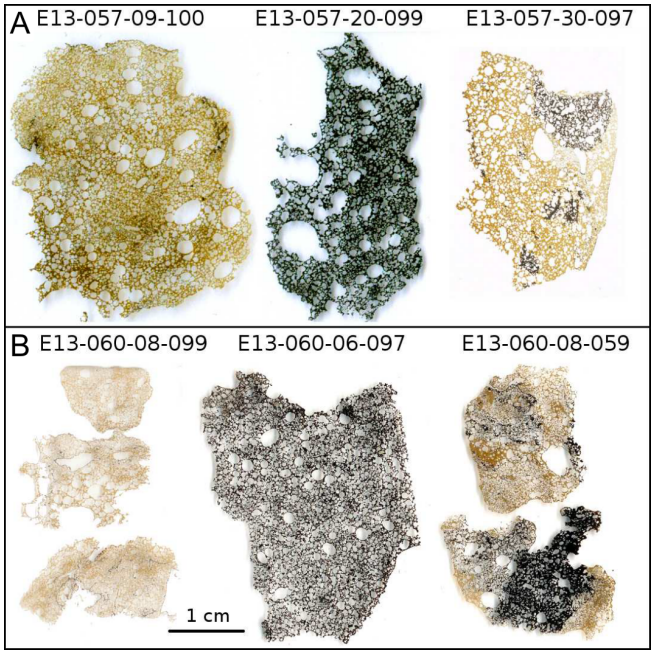

Figure 8: Example thin-sections of Eldgjá [A] magmatic and [B] phreatomagmatic pyroclasts. Both eruption style end-members exhibit both microlite-poor (golden) and microlite-rich (black) domains. With the exception of E13-060-08-059, all of these clasts have undergone vesicle-size analysis.

4.3 Vesicle textures

Regardless of whether the sample is magmatic or phreatomagmatic, or microlite-rich or -poor, vesicles range from 3 µm to over 250 µm (Figure 9). The smallest vesicles (3–16 µm) appear perfectly round, gradually becoming more elliptical in larger size bins. MRDs tend to contain more of the smallest vesicles (Figure 9J, L). The largest vesicles (> 250 µm) generally, but not always, show morphologies suggesting they grew by the process of coalescence (Figure 12) but there is no textural evidence for widespread vesicle collapse or shear deformation. The walls between vesicles are generally between 10 to 40 µm thick.

In terms of vesicles, the most visually apparent difference between domain types is that vesicles within the MRDs tend to have more ragged outlines (Figure 9J, 9L, 10). Vesicles which straddle the border between two contrasting domains have convolute outlines on margins within the MRD and smooth outlines on edges within the MPD. However, in both domains, the larger vesicles are of overall similar morphology.

In several of the samples strings of vesicles stretch across the thin section at various length scales from several centimetres to microns (Figure 12). The vesicles making up these strings are generally small (30 to 100 µm) although rarely the strings contain smaller vesicles coalescing to form larger vesicles. It is uncommon to find more than one string in a single thin section. The strings are up to 30 mm in length and between 0.2 and 1 mm wide. The strings can be found both cutting through (Figure 12A) and forming along the edges of MRDs (Figure 12B).

4.4 Quantification of Vesicle Textures

Vesicle number densities (N_V) for magmatic and phreatomagmatic tephra clasts are similar, both are in the range 3×10^3 mm^{-3} to 2×10^4 mm^{-3} and when adjusted to account for the volume of the vesicles themselves the corresponding $N_V{}^m$ values are 1×10^4 mm^{-3} to 1×10^5 mm^{-3} (Figure 13, Table 2). The phreatomagmatic samples exhibit a greater range in terms of $N_V{}^m$ values than the magmatic samples, 9.8×10^4 mm^{-3} compared to 4.5×10^4 mm^{-3}, and have a higher average $N_V{}^m$ of 6.1×10^4 mm^{-3} versus 2.8×10^4 mm^{-3}. The MRDs tend to have higher $N_V{}^m$ values although there is some overlap (Figure 13).

Vesicle volume distributions (Figure 14) are histograms showing the volume fraction contributed by each vesicle size bin. The Eldgjá distributions are generally unimodal, although three samples (E13-057-14-098 and E13-057-20-099, both magmatic; and E13-060-08-099, phreatomagmatic) have an additional coarse mode. The majority of the distributions are log-symmetric or slightly negatively-skewed with the exception of four samples (E13-057-09-100, E13-057-20-099, E13-057-26-096, magmatic; and E13-060-08-099, phreatomagmatic) which are slightly positively-skewed. Two of these positively-skewed distributions also show an additional coarse mode. The modes of all but one sample are between 0.16 and 0.41 mm (Figure 14); E13-060-08 has a slightly finer mode between 0.13 and 0.16 mm. The median bubble size for all samples is between 0.16 and 0.31 mm.

Cumulative vesicle volume curves (Figure 15A and B) allow direct comparison of multiple samples which can be difficult in vesicle volume distributions. The cumulative vesicle volume curves show no systematic differences between microlite-poor and -rich samples (Figure 15A). The phreatomagmatic samples show a greater contribution from small vesicles than do the magmatic samples (Figure 15B).

As the Skælingar section contains several samples from the same eruptive unit (E13-057-09 to E13-057-20), these distributions allow an examination of the degassing processes through time (Figure 16). These distributions are very similar however there are some nuances. The lower-most sample shows a lower contribution from the smallest vesicles. The upper-most sample shows a shallower slope indicating a greater contribution from larger vesicle size-fractions. The two samples which show additional coarse modes in the vesicle size distributions (E13-057-14-098 and E13-057-20-099) are easily identifiable in the cumulative curves, showing sharp up-turns at the largest vesicle sizes.

In order to quantify the similarity of the vesicle vol-

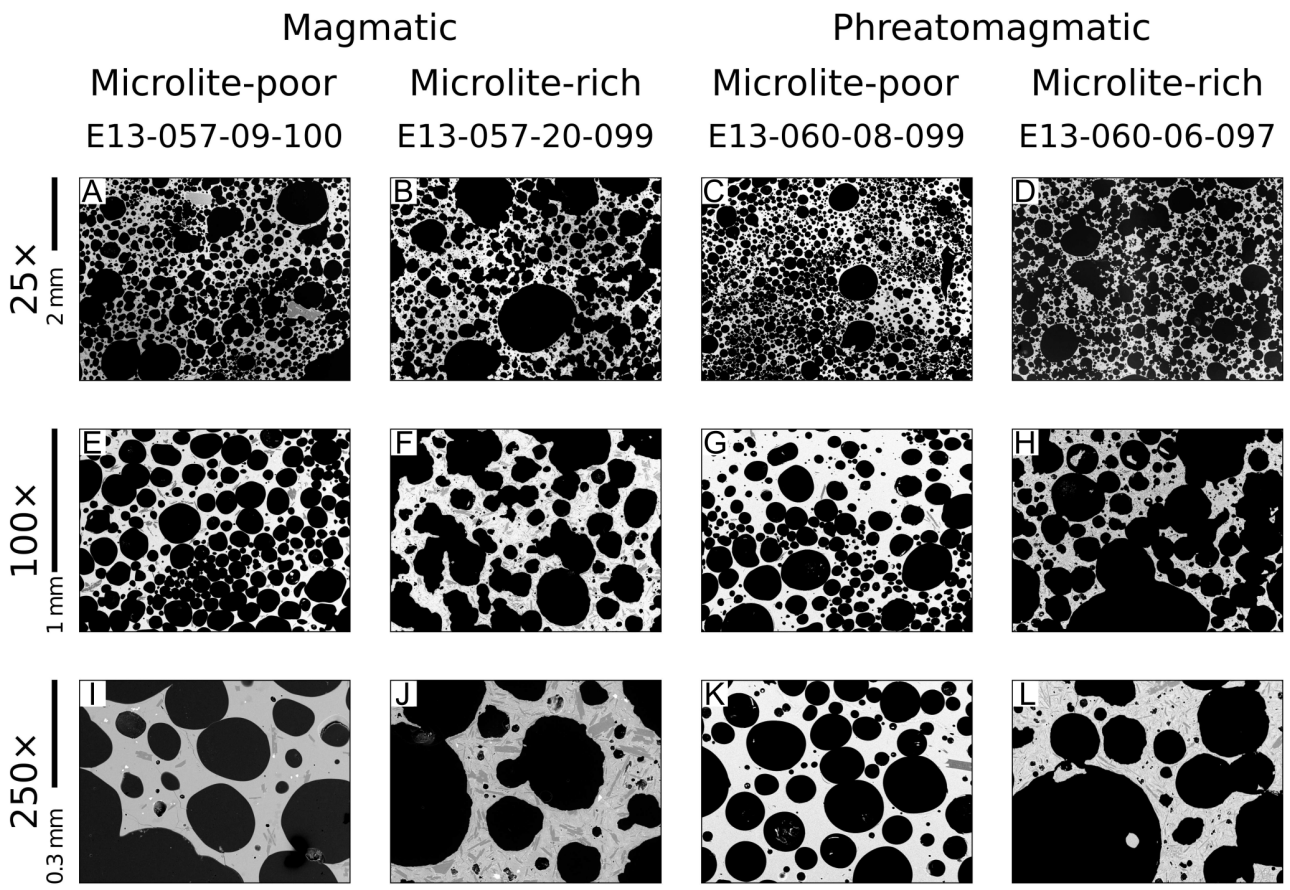

Figure 9: Example images of Eldgjá tephra under a scanning electron microscope at 25×, 100×, and 250× magnification. Both magmatic and phreatomagmatic examples are shown, each with an example of microlite-poor, and -rich pyroclasts.

ume distributions a two-sample Kolmogorov–Smirnov test was used, the results of which are presented in Figure 14 as a matrix of p-values. As none of the p-values are less than 0.1, the null hypothesis (that the distributions of each tested pair are identical) cannot be rejected.

A weakness of vesicle volume distributions is that the volume-contribution from the smallest vesicles is almost negligible and so even a large number of these vesicles will have little effect on the shape of the distribution. The vesicle number density does not have this problem and so a plot of vesicle-to-melt ratio (V_g/V_l after Gardner et al. [1996]) and vesicle number density can be used to identify trends at all scales (Figure 15C and D, after Stovall et al. [2011]). Whilst there is some overlap between the microlite-poor and microlite-rich samples, the former have fewer bubbles than the latter (Figure 15C). Given that the vesicle volume distributions of both domain types are so similar, this difference in vesicle number must arise from the smallest vesicle size-fractions. Both domain types have similar V_g/V_l ratios, reiterating that there is little, if any, difference between the microlite-poor and -rich clasts in terms of those large vesicles which contribute most to bulk volume. The mixed clasts exhibit almost the entire range of vesicle number densities and V_g/V_l ratios. There is even less difference between the samples when grouped into magmatic or phreatomagmatic type (Figure 15D). As was seen in Figure 13, the phreatomagmatic samples have higher number densities than the magmatic samples but there is significant overlap.

5 Interpretation

5.1 Clast density and bulk vesicularity

The magmatic tephra reveal tight, unimodal vesicularity/density distribution compared to the phreatomagmatic tephra (Figure 6 and 7). The Skælingar tephra also have slightly lower average vesicularities than Stóragil irrespective of whether the latter are magmatic or phreatomagmatic.

The tight magmatic vesicularity distributions (Figure 7) are strongly suggestive of a single fragmentation mechanism, to be expected if the expansion of ex-

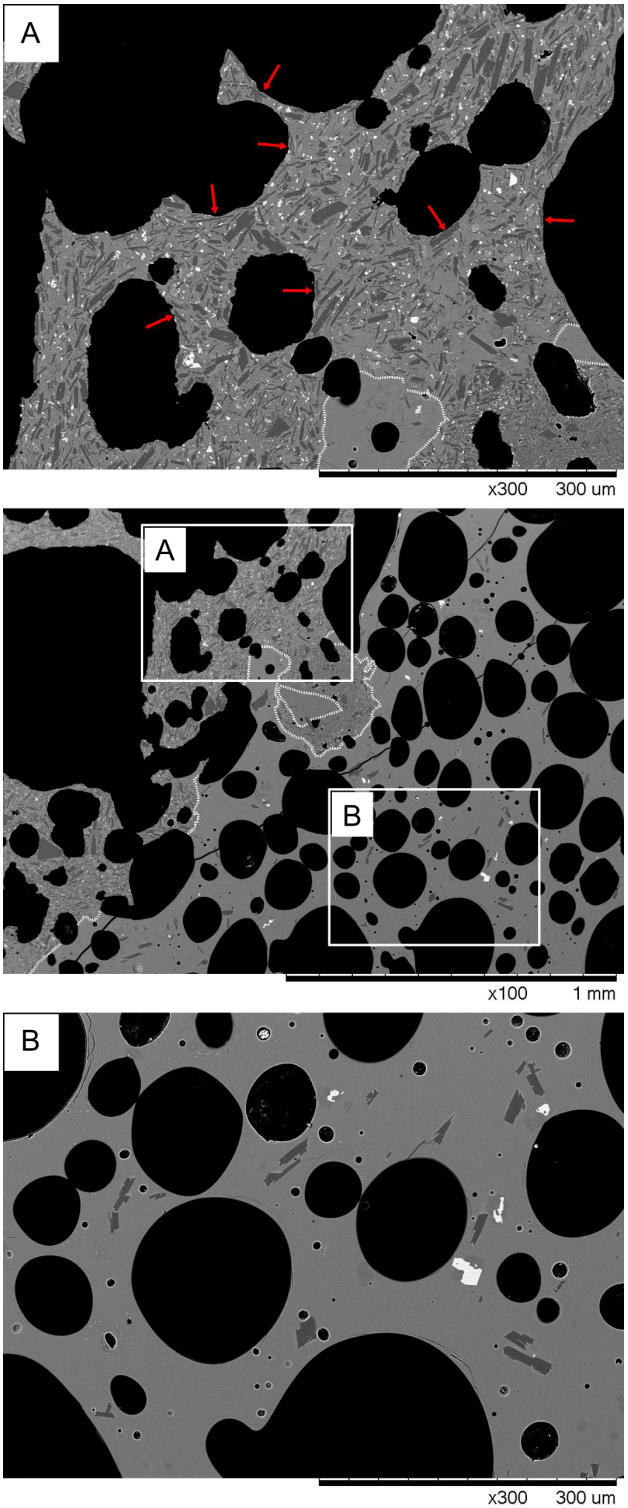

Figure 10: Microlite-rich versus -poor domains within a single pyroclast (E13-057-30-097). The microlite-rich domains [A] contain over 30 % microlites by area but have similar vesicle size distributions to the microlite-poor domains [B]. Red arrows in [A] point to microlites which appear to have aligned with the bubble edges during bubble growth.

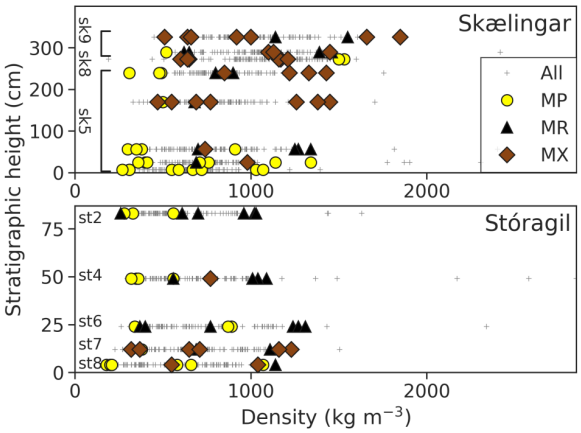

Figure 11: Plots of density against stratigraphic height for the two key tephra sections. Grey crosses indicate density measurements of individual clasts from each sampled horizon whilst MP, MR, and MX refer to microlite-poor, microlite-rich, and clasts containing both domains respectively.

solved magmatic gases [Houghton and Wilson 1989] is the controlling factor in driving the magma to fragmentation. This would occur at some critical vesicularity threshold (50 to 70 % in basaltic magmas; Swanson [1973]) and fragmentation would cause the abrupt cessation of bubble nucleation and growth.

The phreatomagmatic tephra exhibit relatively broad, plateau-like vesicularity distributions (Figure 6 and 7, Table 2). That being said, with the exception of the top four samples from Skælingar, the phreatomagmatic samples have similar modes to the magmatic samples, albeit not as sharp. This indicates that the bulk of the magma erupting during these phreatomagmatic episodes exemplifies magma that had fully degassed at 1 atmosphere (i.e. surface conditions). In other words, it had vesiculated fully before coming into contact with external water.

5.2 Qualitative microtextural observations

Two microlite size populations are present in the Eldgjá tephra, the smaller of which dominate the MRDs which form entire pyroclasts or exist as enclaves within MPDs. The coarser size-fraction is present in both MPDs and MRDs and this is taken as evidence that the two domains were once texturally identical.

The convoluted nature of the contact between the domains seen in the mixed-type clasts, and the fact that growing bubbles cross the contact (Figure 10), indicates that the domains were both fluid at the time of mingling. Additionally, microlites within MRDs are seen aligned with vesicle walls or occasionally, when perpendicular to vesicle walls, deforming those walls (Figure 10). This suggests that the microlites in the MRDs had formed prior to final bubble growth. Be-

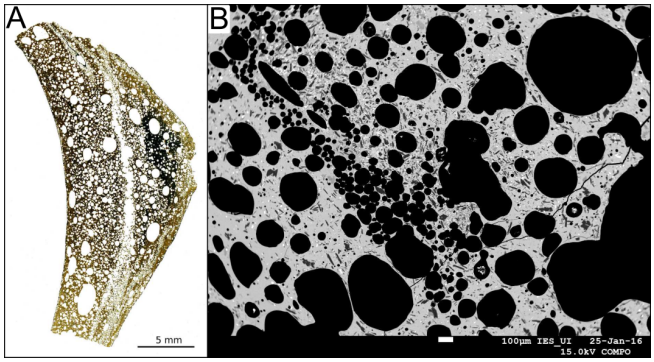

Figure 12: Two examples of vesicle strings at two different scales: [A] scanned image of thin section E13-057-26-097 showing a coalesced vesicle string along the length of the pyroclast of width 1 mm and length > 29 mm; [B] Electron microprobe image showing fine-scale vesicle string of width 0.23 mm and length > 2.33 mm consisting of vesicles between 30 and 100 µm.

cause lapilli-sized clasts are capable of preserving complex contacts between domain types, the contacts must have been convoluted on the centimetre-scale. Additionally, these contacts must have remained sharp given the lack of samples recording textures transitional between the two domain types.

The units sampled at Skælingar were erupted from a single short length of fissure and together provide a record of evolving microlite textures through time. The units sampled at Stóragil were erupted from many different parts of the fissure and as such are a record of processes affecting the magma being supplied to the fissure as a whole. The Skælingar samples show a clear increase in the amount of MRDs and mixed clasts with time whilst the Stóragil samples show no correlation (Figure 11). This indicates that the process producing MRDs occurs locally at each fissure segment.

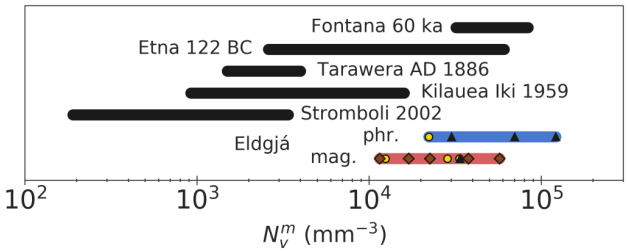

Figure 13: Eldgjá magmatic and phreatomagmatic vesicle number densities ($N_V{}^m$) compared with those of other basaltic eruptions determined by the same methods: Fontana 60 ka [Costantini et al. 2010]; Etna 122 BCE [Sable et al. 2006]; Tarawera 1886 [Sable et al. 2009]; Kilauea Iki 1959 Episode 1 [Stovall et al. 2011]; and Stromboli 2002 [Lautze and Houghton 2007]. Symbols as in Figure 11.

5.3 Quantitative vesicle data

In Figure 13 we compare the vesicle number densities with other known basaltic explosive eruptions, quantified by the same methods, namely: the Plinian episodes of Fontana 60 ka [Costantini et al. 2010], the Plinian episodes of Etna 122 BCE [Sable et al. 2006], Tarawera 1886 [Sable et al. 2009], Episode 1 of Kilauea Iki 1959 [Stovall et al. 2011], and Stromboli 2002 [Lautze and Houghton 2007]. These comparisons show that Eldgjá vesicle number densities fall on the higher end of the intensity spectrum and are comparable with those of the basaltic Plinian eruptions of Etna 122 BCE and Fontana 60 ka.

High vesicle number density values have been linked to rapid magma ascent rates [Houghton and Gonnermann 2008] which are to be expected with any powerful explosive basaltic eruption where high ascent rates are required to keep the volatile and melt phases coupled. Studies of basaltic pyroclastic systems have demonstrated that vesicle number density is proportional to eruption intensity [Polacci et al. 2006; Sable et al. 2006; Stovall et al. 2012]. Our results imply that individual explosive episodes during the Eldgjá flood lava eruption had similar intensities to some of the most powerful basaltic explosive eruptions known.

5.4 Vesicle volume distributions

Both the magmatic and phreatomagmatic clasts present unimodal vesicle volume distributions (Figure 14) indicating single nucleation events. The majority of the samples are either log-symmetric, or slightly negatively-skewed which indicate continuous nucleation events which were still ongoing until the clasts were quenched. Several of the samples show either positively-skewed distributions or additional coarse modes. This is interpreted as recording a history of coalescence.

The difference between MRDs and MPDs, in terms of vesicles, is restricted to the abundance of the smallest vesicles (Figure 15C and D). This slight difference limits the relative timing of MRD formation to after the start of vesicle nucleation.

6 Discussion

6.1 Role of external water in the eruption

The explosive episodes of Eldgjá provide the perfect opportunity to examine the role of water during a subglacial eruption because: 1) activity took place at both subglacial and subaerial vents and; 2) the magma composition remained relatively constant throughout the eruption.

The magmatic tephra deposits are evidence that 58 to 80 % of vesiculation was capable of fragmenting the

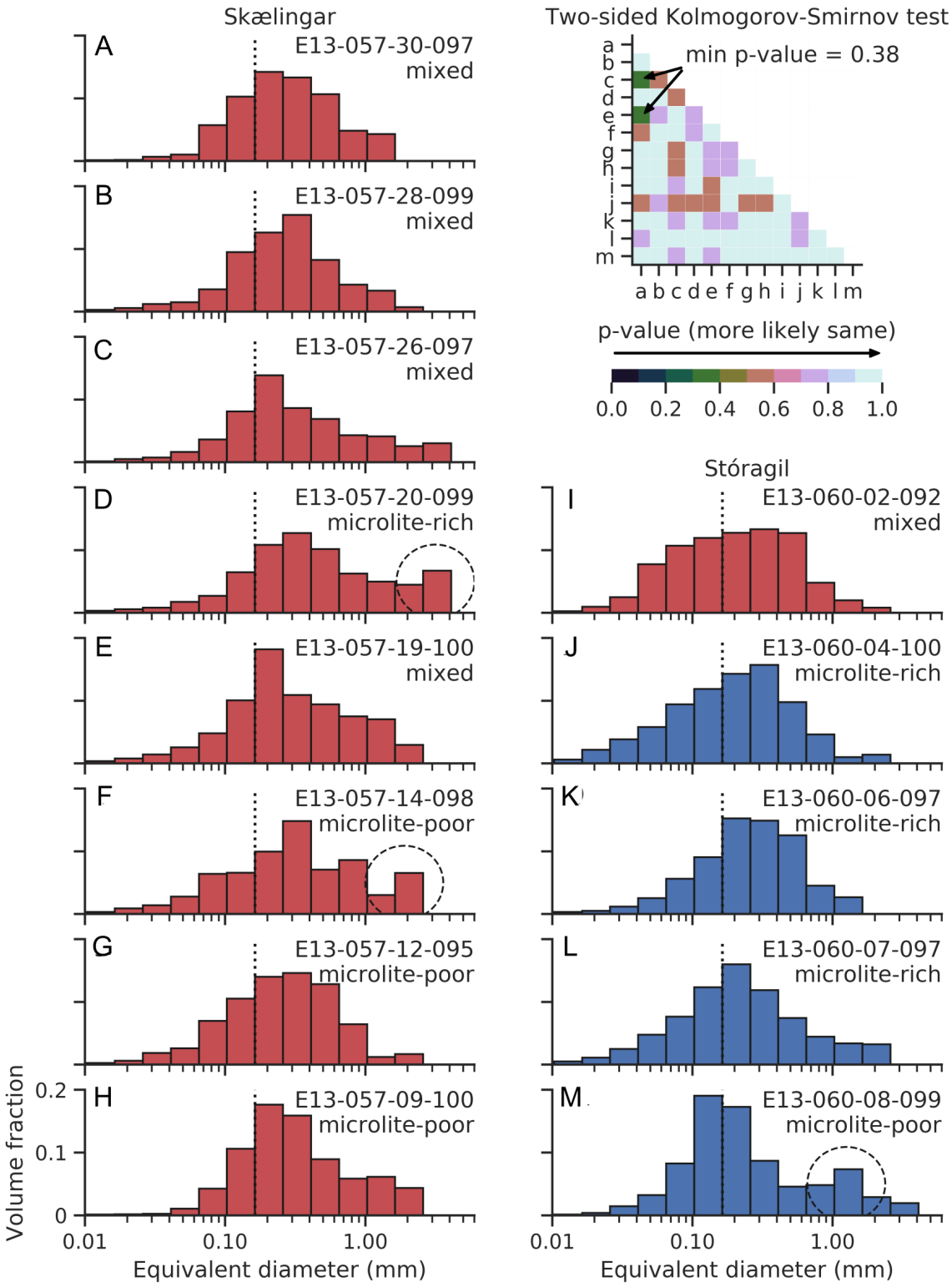

Figure 14: Vesicle volume distributions for the Skælingar and Stóragil tephra sections. Red plots are magmatic samples and blue phreatomagmatic. Each plot is labelled with the sample number and whether the sample is microlite-poor, -rich, or mixed. Dashed black circles highlight additional coarse modes. The black dotted line is to aid comparison between distributions and is located at 0.16 mm equivalent diameter. Inset is a matrix of results from a series of Kolmogorov–Smirnov tests; a p-value less than 0.1 is needed to be confident that the distributions are statistically different. The lighter the colour, the more likely the distributions are the same. None of the p-values are less than 0.1 and so the distributions are statistically similar.

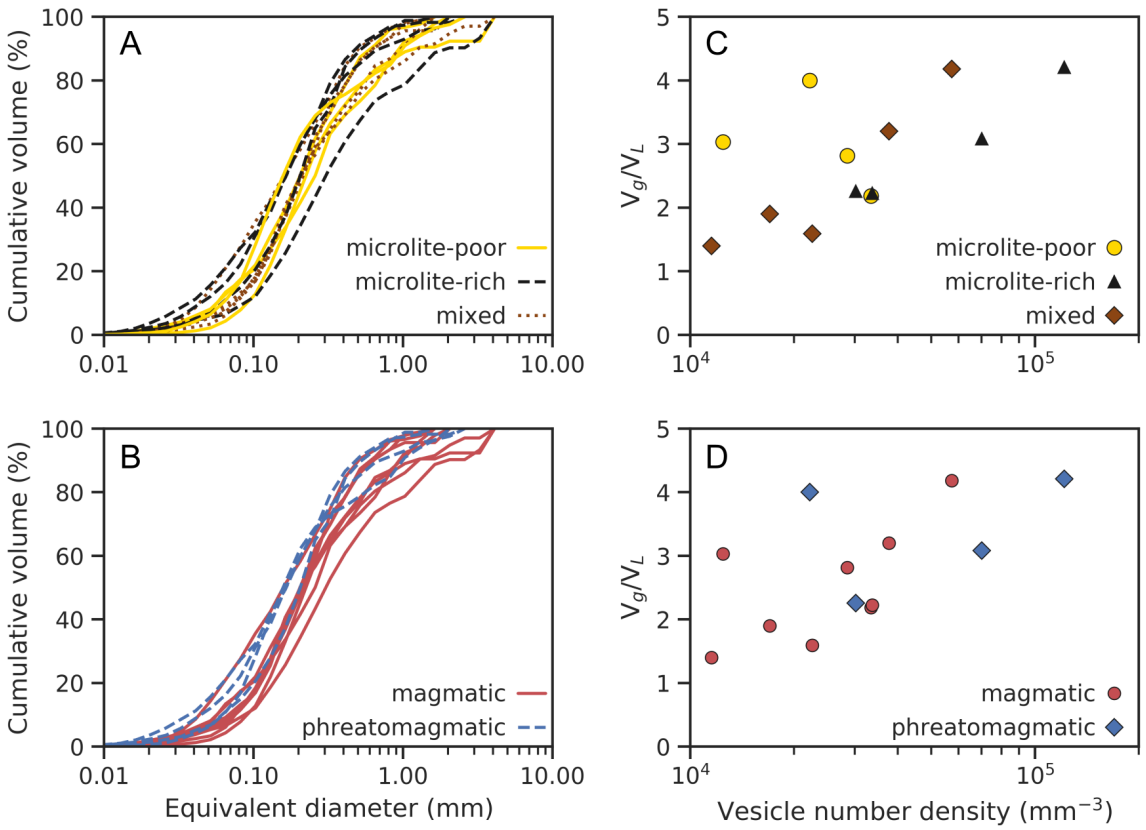

Figure 15: [A] Cumulative vesicle volume distributions of each of the samples shown in Figure 14, colour and line style correspond to microlite texture of sample. [B] CVVD for the same samples this time grouped into magmatic and phreatomagmatic. [C] Ratio of vesicle volume to melt (V_g/V_l) against vesicle number density ($N_V{}^m$) with samples grouped as in [A]. [D] Same as [C] but grouped into magmatic and phreatomagmatic.

magma explosively at the subaerial vents. The vesicle-size analyses have demonstrated that the history of vesicle nucleation, growth, and coalescence was essentially identical for the magmas that were erupted at subglacial and subaerial vents (Figure 14, 15). From these two observations it is clear that the magma at the subglacial vents was also capable of fragmenting explosively entirely as a consequence of exsolution and expansion of the magmatic volatiles.

However, given that the magmatic and phreatomagmatic tephra deposits have very different grain-size distributions (Figure 5), external water must have had some role in processes taking place in the subglacial vents. The tephra produced from subaerial vents contain many achneliths, indicative of fragmentation in a hot vent environment [Walker and Croasdale 1971]. Whilst the tephra produced from subglacial vents lack achneliths, the clasts do not exhibit the features typical of phreatomagmatic fragmentation, such as quenching cracks, on a microscopic scale (Figure 4B; Zimanowski et al. [2015]).

The textural evidence indicates that the magma had vesiculated at least to the point of foam by the time external water became involved. Thermohydraulic explosions require that two immiscible liquids meet in

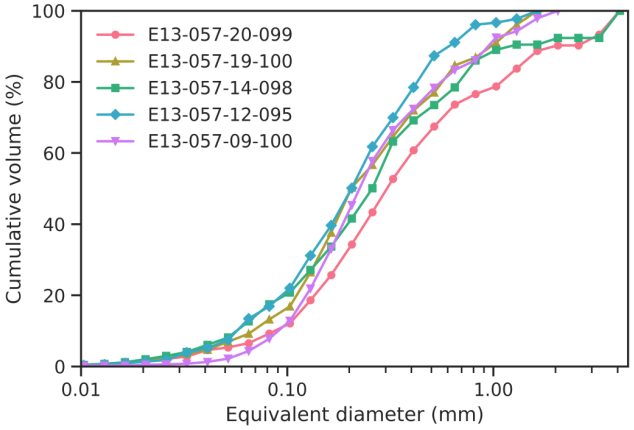

Figure 16: Cumulative vesicle volume distribution showing samples from Skælingar which were erupted from the same episode (sk5; Figure 6). The legend is in stratigraphic order.

a premix-phase [Wohletz 1983]. Vesiculated foam has much higher yield strength than non-vesicular magma [Höhler and Cohen-Addad 2005] and so fuel–coolant interactions are less likely to occur. An alternative process is thermal granulation of the foam via quench-

ing, forming fine-scale hydro-fractures within the pyroclasts, which partly or wholly disintegrated to form the ash. This kind of process does not add any explosivity to the system [Kokelaar 1986] but modifies the grain-size distribution to finer size-fractions. So whilst the subglacially-derived tephra was at least partially fragmented by magma–water interaction, it was at the low-energy end of the phreatomagmatic spectrum. Thermal energy is transferred more efficiently from finer-grained material and so one implication of thermal-granulation is hotter and therefore more buoyant volcanic plumes.

Eruptions at the subglacial segments of Eldgjá would have initially produced ice-cauldrons (depressions on the ice surface) as during the 2014 Holuhraun eruption [Reynolds et al. 2017] which would progress to fully open chasms as during the 1996 Gjálp eruption [Gudmundsson et al. 2004]. Water would have been available for phreatomagmatic processes throughout these stages of the eruption, either in the form of ice-bound ponds or water-saturated bedrock. No evidence has been found for the total consumption of water at the subglacial vents. At the glacier margin where the ice is thinnest, the ice would have been removed most rapidly. Future work is needed to examine the transitional vent processes which took place in this region of the fissure system.

More work, particularly experimental work, needs to be carried out to fully understand the processes involved when an unstable, fragmenting foam at magmatic temperatures meets external water at ambient temperatures. It is hard to envisage a sufficient premix-phase forming when one of the liquids is a highly vesiculated foam. The results from such work would have widespread implications as it is not an uncommon situation: for example, the wet phases of the silicic 1875 eruption of Askja, Iceland, was found to have involved a highly vesicular foam meeting external water [Carey et al. 2009] which was stored in pristine and highly permeable lavas at the surface [Lupi et al. 2011].

6.2 Origin of microlite domains

Previous work has found MRDs to arise in several different settings. These include:

1. during the drain-back of material within a lava lake into the conduit or storage setting [e.g. Stovall et al. 2012];

2. the passage of small (normal Strombolian) or large (Strombolian paroxysms) volumes of hot, microlite-poor, vesicular magma accompanying large, decoupled bubbles into stagnant, cooler, and more microlite-rich melt in the uppermost conduit [e.g. Cimarelli et al. 2010; Lautze and Houghton 2005];

3. the development of concentrically zoned shells of magma of contrasting textures in the shallow conduit as the result of a Gaussian velocity profile and hence contrasting ascent rates between the axis and the margin of the conduit as interpreted for some basaltic Plinian events [e.g. Costantini et al. 2010];

4. as the dyke of an erupting fissure narrows to one or more point source vents, progressive storage of melt in inactive portions of the upper dyke leads to localised lateral drainage of the cooler, stored melt towards the still-erupting vents and mingling with the newly arrived, hotter melt [e.g. Murtagh and White 2013].

The Eldgjá microlite and vesicle textures show both similarities and significant differences with observations made of eruptions from these various settings. A common observation in all of these cases is poly-lobate or amoeboidal vesicle shapes in MRDs. This is often accompanied by rough vesicle edges caused by the contact of the vesicle with microlites, as seen in the Eldgjá tephra, which has been interpreted as evidence of contemporaneous growth of bubbles and microlites [Costantini et al. 2010].

In both Strombolian-style and more powerful explosions, studies have found MPDs to have bimodal or polymodal vesicle-size distributions [Costantini et al. 2010; Lautze and Houghton 2005]. This contrasts with the Eldgjá data which show unimodal distributions regardless of microlite content.

Another major difference between observations of subplinian-Plinian and Eldgjá is the lack of mingled textures in the former. Both the Fontana Lapilli [Costantini et al. 2010] and Etna 122 BCE [Sable et al. 2006] basaltic Plinian eruptions exhibit clasts which are either microlite-poor or -rich but no clasts which feature both. This does not mean mingling did not take place but could represent the size of domains. Both the Fontana Lapilli and 122 BCE eruptions erupted through cylindrical-like conduits in contrast to the dykes which fed the Eldgjá eruption. Given that, for a set cross-sectional area, the ratio of perimeter to area is always lower in cylindrical-like conduits than dyke-like, there will be more opportunity in dyke-like conduits for mingling of a hotter, microlite-poor core with a cooler, microlite-rich margin.

The microlite and vesicle textures seen in clasts formed by the eruption of a Hawaiian fire-fountain through a lava lake [Stovall et al. 2012] are extremely similar to those seen in the Eldgjá tephra. However, the mingled microlite textures found in the Eldgjá tephra originate from multiple locations along the subglacial and subaerial fissure segments and at least 16 individual explosive episodes (Figure 3). If the mingling of MPDs and MRDs originated solely from recycling then lava lakes were not likely to be involved.

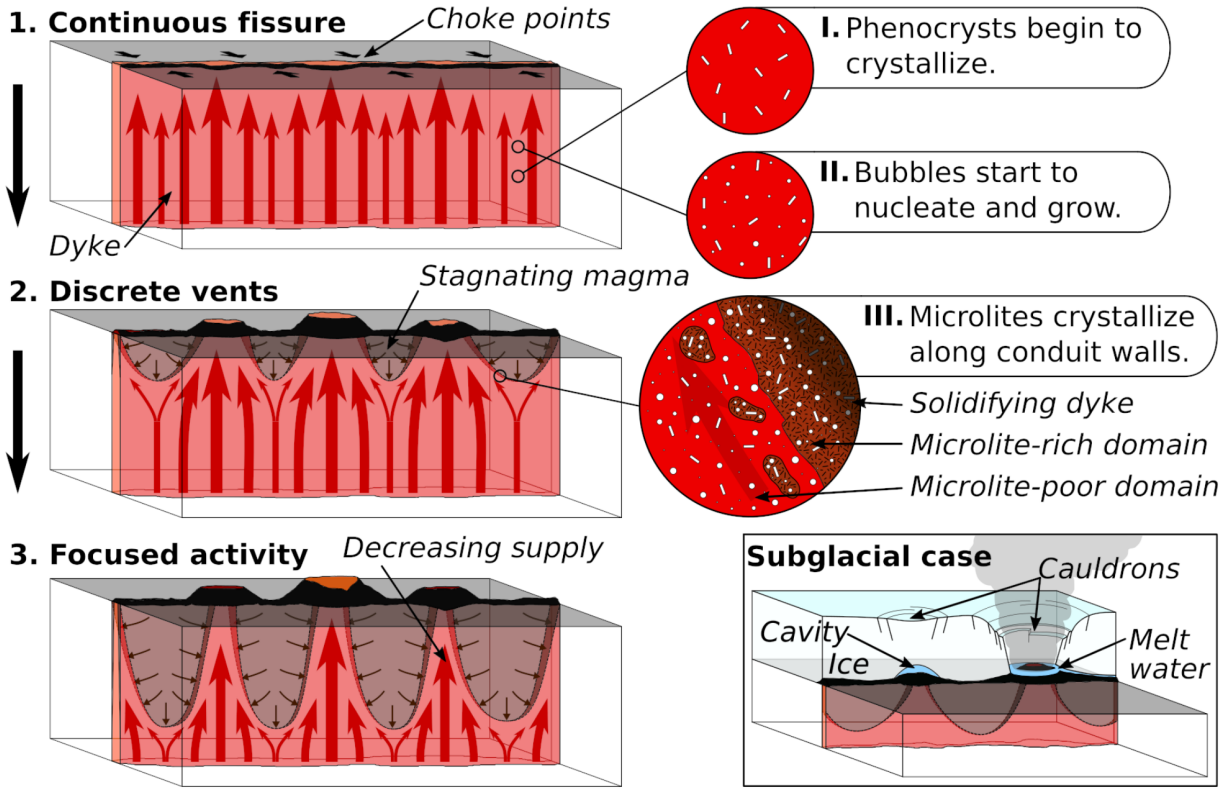

Figure 17: Schematic diagrams outlining the model of fissure focus and textural evolution of the magma: 1) Magma ascends vertically through a sheet-like conduit. Plagioclase phenocrysts crystallize first (I), followed at a shallower depth by the first nucleation of bubbles (II). 2) A combination of volatile exsolution and heat-loss to the country-rock starts microlite crystallization which, combined with initial heterogeneity in dyke width, leads to progressive closing of the conduit and focusing of magma flow to wider segments of the dyke. Portions of the microlite-rich material along the conduit walls are incorporated into erupted material by magma flow and recorded as microlite-rich versus -poor domains (III). 3) Eruptive activity decreases and eventually ceases at vents depending on magma supply. The subglacial fissure segments create surface expressions dependant on the volume of magma reaching the surface and the corresponding heat-flow.

The fourth scenario presented above is more plausibly invoked at all or a majority of the Eldgjá fissure segments. A common observation in fissure eruptions is an initially continuous linear vent which quickly focuses down to one or two shorter or point-source vents (e.g. the 2014-15 Holuhraun eruption; Pedersen et al. [2017]). A combination of irregularities in the initial geometry of the fissure [Ida 1992] and heat-loss to the country-rock [Bruce and Huppert 1989; Delaney and Pollard 1982; Wylie et al. 1999] produce feedback loops wherein narrower parts of the fissure or lengths with lower magma flux experience increased cooling and microlite growth, increasing the magma viscosity in these regions and so further lowering flux and width of the dyke. Lava from these segments may then flow laterally and mingle with microlite-poor magma in the wider and still-active parts of the fissure.

6.3 A model of shallow conduit processes

A model of the processes which were active in the shallow conduit during the Eldgjá eruption is presented, based on the evidence provided by vesicle and microlite textures and is outlined in Figure 17.

The magma ascending beneath subglacial and subaerial fissure segments of Eldgjá was initially physically identical. Rapidly ascending magma began to crystallize the larger plagioclase laths. The rapid ascent of the magma led to volatile supersaturation and the homogeneous nucleation of bubbles.

The combination of volatile exsolution and heat-loss along the conduit margins resulted in undercooling and onset of crystallization at the margins. A convoluted interface between microlite-rich and -poor material was a source of microlite-rich material which was incorporated into the magma being supplied to the surface and recorded as MRDs versus MPDs in the tephra.

The region of more microlite-rich material progressively controlled the flow of magma within the dyke—both in the vertical and, eventually, lateral dimensions.

This process is, along with initial heterogeneity of the fissure, what controlled the transition from a semi-continuous curtain of fire from a sheet-like conduit to focused activity at discrete vents fed by more pipe-like conduits. Similar processes have been inferred to have occurred in other Icelandic [Eibl et al. 2017; Witt et al. 2018] and Hawaiian eruptions [Parcheta et al. 2015].

7 Conclusions

Explosive episodes during the 10th century Eldgjá fissure eruption were characterized by late-stage, rapid nucleation of bubbles regardless of whether the fissure segment in question was subglacial or subaerial. With respect to the subglacial explosive episodes, fragmentation due to exsolution of magmatic volatiles was probably already underway prior to the involvement of external water. The role of this water in fragmentation was then limited to secondary thermal granulation of an already disrupting magma. This is inconsistent with the popular view that explosive basaltic volcanism in Iceland is dominantly driven by explosive magma–water (i.e. fuel–coolant like) interactions. The results presented here demonstrate that explosive activity in both the dry and the wet situations is driven by the exsolution and explosive expansion of magmatic gases. The implication of this is that explosive magma–water interactions can not be assumed in all Icelandic subglacial eruptions.

Microlite textures within the tephra record a complex history of mingling of domains of microlite-rich and -poor material. A model of changing conduit geometry, from dyke-like to pipe-like, is proposed based upon the textural evidence and application of the results of previous research. The complex microlite textures are found in most Eldgjá tephra and so this conduit model is likely common to every part of the fissure system, both subglacial and subaerial.

Acknowledgements

This work was supported by the Icelandic Research Fund, Rannís (PhD grant no. 121116-0061) and the South Iceland Research Fund, Vísinda- og Rannsóknarsjóðs Suðurlands. A special thanks to Catherine Gallagher, Jónas Guðnason, Maria Janebo, Delphine Klaessens, Darrell Knight, Christopher Lofthouse, Richard Moreland, and Hannah Reynolds for assistance in the field; to Hannah Reynolds for proofreading; and Tobias Dürig, Jacqueline Owen, and Hugh Tuffen for fruitful discussions on subglacial volcanism. An earlier version of this manuscript benefited from comments by Corrado Cimarelli, Valentin Troll, Sebastian Watt and an anonymous reviewer. This version has been significantly improved by comments from Julia Eychenne, editor Ulrich Küppers and an anonymous reviewer.

Author contributions

WMM carried out the fieldwork, lab analyses, and interpretation as part of his PhD at the University of Iceland under the supervision of TT, BFH, and GL. WMM and TT were involved in acquisition of data whilst GL advised on field localities and interpretation of depositional units. BFH advised on the application of vesicle analysis techniques and interpretation. WMM drafted the manuscript and all authors have read and approved it.

Data availability

The Python script used to process the vesicle measurements is available on GitHub and Zenodo [Moreland 2019] and the vesicle area data is available through Zenodo [Moreland et al. 2019]. Additional isopach data is given in Supplementary Material alongside the online version of this article.

References

Aravena, A., M. de'Michieli Vitturi, R. Cioni, and A. Neri (2018). "Physical Constraints for Effective Magma-Water Interaction along Volcanic Conduits during Silicic Explosive Eruptions". *Geology* 46.10, pp. 867–870. issn: 0091-7613. doi: 10/gfcv82.

– (2019). "Physical Constraints for Effective Magma-Water Interaction along Volcanic Conduits during Silicic Explosive Eruptions: REPLY". *Geology* 47.5, e462–e462. doi: 10/c839.

Baillie, M. G. L. and J. McAneney (2015). "Tree Ring Effects and Ice Core Acidities Clarify the Volcanic Record of the First Millennium". *Clim. Past* 11.1, pp. 105–114. doi: 10/f6x2cw.

Bottinga, Y. and D. F. Weill (1970). "Densities of Liquid Silicate Systems Calculated from Partial Molar Volumes of Oxide Components". *American Journal of Science* 269.2, pp. 169–182. issn: 0002-9599, 1945-452X. doi: 10/dp55jc.

Bruce, P. M. and H. E. Huppert (1989). "Thermal Control of Basaltic Fissure Eruptions". *Nature* 342.6250, pp. 665–667. doi: 10/fjvpsg.

Büttner, R., P. Dellino, and B. Zimanowski (1999). "Identifying Magma–Water Interaction from the Sur-

face Features of Ash Particles". *Nature* 401.6754, pp. 688–690. DOI: 10/brfbcd.

Carey, R. J., B. F. Houghton, and T. Thordarson (2009). "Abrupt Shifts between Wet and Dry Phases of the 1875 Eruption of Askja Volcano: Microscopic Evidence for Macroscopic Dynamics". *Journal of Volcanology and Geothermal Research* 184.3–4, pp. 256–270. DOI: 10/d9g7wm.

Cimarelli, C., F. D. Traglia, and J. Taddeucci (2010). "Basaltic Scoria Textures from a Zoned Conduit as Precursors to Violent Strombolian Activity". *Geology* 38.5, pp. 439–442. DOI: 10/fgdpkb.

Colombier, M., B. Scheu, U. Kueppers, S. J. Cronin, S. B. Mueller, K.-U. Hess, F. B. Wadsworth, M. Tost, K. J. Dobson, B. Ruthensteiner, and D. B. Dingwell (2019). "In Situ Granulation by Thermal Stress during Subaqueous Volcanic Eruptions". *Geology*. DOI: 10/gfth7t.

Costantini, L., B. F. Houghton, and C. Bonadonna (2010). "Constraints on Eruption Dynamics of Basaltic Explosive Activity Derived from Chemical and Microtextural Study: The Example of the Fontana Lapilli Plinian Eruption, Nicaragua". *Journal of Volcanology and Geothermal Research* 189.3–4, pp. 207–224. DOI: 10/bmrhq6.

Delaney, P. T. and D. D. Pollard (1982). "Solidification of Basaltic Magma during Flow in a Dike". *American Journal of Science* 282.6, pp. 856–885. DOI: 10/fc7vgs.

Eibl, E. P. S., C. J. Bean, I. Jónsdóttir, A. Höskuldsson, T. Thordarson, D. Coppola, T. Witt, and T. R. Walter (2017). "Multiple Coincident Eruptive Seismic Tremor Sources during the 2014–2015 Eruption at Holuhraun, Iceland". *Journal of Geophysical Research: Solid Earth* 122.4, pp. 2972–2987. ISSN: 2169-9356. DOI: 10/f9899b.

Gardner, J. E., R. M. E. Thomas, C. Jaupart, and S. Tait (1996). "Fragmentation of Magma during Plinian Volcanic Eruptions". *Bulletin of Volcanology* 58.2-3, pp. 144–162. DOI: 10/bc3s66.

Gislason, S. R. et al. (2011). "Characterization of Eyjafjallajökull Volcanic Ash Particles and a Protocol for Rapid Risk Assessment". *Proceedings of the National Academy of Sciences* 108.18, pp. 7307–7312. DOI: 10/bswrcg.

Gonnermann, H. M. (2015). "Magma Fragmentation". *Annual Review of Earth and Planetary Sciences* 43.1, pp. 431–458. DOI: 10/gdh7xd.

Grönvold, K., N. Óskarsson, S. J. Johnsen, H. B. Clausen, C. U. Hammer, G. Bond, and E. Bard (1995). "Ash Layers from Iceland in the Greenland GRIP Ice Core Correlated with Oceanic and Land Sediments". *Earth and Planetary Science Letters* 135.1–4, pp. 149–155. ISSN: 0012-821X. DOI: 10/db2dzt.

Gudmundsson, M. T., F. Sigmundsson, H. Björnsson, and T. Högnadóttir (2004). "The 1996 Eruption at Gjálp, Vatnajökull Ice Cap, Iceland: Efficiency of Heat Transfer, Ice Deformation and Subglacial Water Pressure". *Bulletin of Volcanology* 66.1, pp. 46–65. DOI: 10/b892tz.

Gudmundsson, M. T. et al. (2012). "Ash Generation and Distribution from the April-May 2010 Eruption of Eyjafjallajökull, Iceland". *Scientific Reports* 2, p. 572. DOI: 10/c3g5.

Hammer, C. U. (1984). "Traces of Icelandic Eruptions in the Greenland Ice Sheet". *Jökull* 34, pp. 51–65.

Hammer, C. U., H. B. Clausen, and W. Dansgaard (1980). "Greenland Ice Sheet Evidence of Post-Glacial Volcanism and Its Climatic Impact". *Nature* 288.5788, pp. 230–235. DOI: 10/bg5q9t.

Höhler, R. and S. Cohen-Addad (2005). "Rheology of Liquid Foam". *Journal of Physics: Condensed Matter* 17.41, R1041. DOI: 10/bsrmtr.

Houghton, B. F. and R. J. Carey (2019). "Physical Constraints for Effective Magma-Water Interaction along Volcanic Conduits during Silicic Explosive Eruptions: COMMENT". *Geology* 47.5, e461–e461. ISSN: 0091-7613. DOI: 10/c84b.

Houghton, B. F. and H. M. Gonnermann (2008). "Basaltic Explosive Volcanism: Constraints from Deposits and Models". *Chemie der Erde - Geochemistry* 68.2, pp. 117–140. DOI: 10/bk264m.

Houghton, B. F. and C. J. N. Wilson (1989). "A Vesicularity Index for Pyroclastic Deposits". *Bulletin of volcanology* 51.6, pp. 451–462. DOI: 10/dhnt99.

Ida, Y. (1992). "Width Change of a Planar Magma Path: Implication for the Evolution and Style of Volcanic Eruptions". *Physics of the Earth and Planetary Interiors* 74.3, pp. 127–138. DOI: 10/drc3vp.

Janebo, M. H., T. Thordarson, B. F. Houghton, C. Bonadonna, G. Larsen, and R. J. Carey (2016). "Dispersal of Key Subplinian–Plinian Tephras from Hekla Volcano, Iceland: Implications for Eruption Source Parameters". *Bulletin of Volcanology* 78.10, p. 66. ISSN: 0258-8900, 1432-0819. DOI: 10/gfs7hm.

Jóhannesson, H., S. P. Jakobsson, and K. Sæmundsson (1990). *Geological Map of Iceland, Sheet 6, South-Iceland*. Reykjavik.

Jones, E., T. Oliphant, P. Peterson, et al. (2001). *SciPy: Open source scientific tools for Python*.

Kokelaar, P. (1986). "Magma-Water Interactions in Subaqueous and Emergent Basaltic Volcanism". *Bulletin of Volcanology* 48.5, pp. 275–289. DOI: 10/cfr2fc.

Langmann, B., A. Folch, M. Hensch, and V. Matthias (2012). "Volcanic Ash over Europe during the Eruption of Eyjafjallajökull on Iceland, April–May 2010". *Atmospheric Environment* 48, pp. 1–8. DOI: 10/crmnmk.

Larsen, G. (2000). "Holocene Eruptions within the Katla Volcanic System, South Iceland: Characteristics and Environmental Impact". *Jökull* 49, pp. 1–28.

Lautze, N. C. and B. F. Houghton (2005). "Physical Mingling of Magma and Complex Eruption Dynamics in the Shallow Conduit at Stromboli Volcano, Italy". *Geology* 33.5, pp. 425–428. DOI: 10/b234hf.

– (2007). "Linking Variable Explosion Style and Magma Textures during 2002 at Stromboli Volcano, Italy". *Bulletin of Volcanology* 69.4, pp. 445–460. doi: 10/btm2f5.

Lupi, M., S. Geiger, R. Carey, T. Thordarson, and B. Houghton (2011). "A Model for Syn-Eruptive Groundwater Flow during the Phreatoplinian Phase of the 28–29 March 1875 Askja Volcano Eruption, Iceland". *Journal of Volcanology and Geothermal Research* 203.3-4, pp. 146–157. doi: 10/dkh96w.

Mangan, M. T. and K. V. Cashman (1996). "The Structure of Basaltic Scoria and Reticulite and Inferences for Vesiculation, Foam Formation, and Fragmentation in Lava Fountains". *Journal of Volcanology and Geothermal Research* 73.1–2, pp. 1–18. doi: 10/ddqnqb.

Mastin, L. G. et al. (2009). "A Multidisciplinary Effort to Assign Realistic Source Parameters to Models of Volcanic Ash-Cloud Transport and Dispersion during Eruptions". *Journal of Volcanology and Geothermal Research*. Improved Prediction and Tracking of Volcanic Ash Clouds 186.1–2, pp. 10–21. doi: 10/cv3szj.

Miller, D. J. (1989). *The 10th Century Eruption of Eldgjá, Southern Iceland*. Tech. rep. Reykjavík: Nordic Volcanological Institute.

Moreland, W. M. (2019). *VSA Processor (Version v0.1)*. Zenodo. doi: 10/c3g6.

Moreland, W. M., T. Thordarson, B. F. Houghton, and G. Larsen (2019). *Vesicle size analysis dataset of Eldgjá tephra (Version v1.0)*. Zenodo. doi: 10/c3mc.

Murtagh, R. M. and J. D. L. White (2013). "Pyroclast Characteristics of a Subaqueous to Emergent Surtseyan Eruption, Black Point Volcano, California". *Journal of Volcanology and Geothermal Research* 267, pp. 75–91. doi: 10/f5jr9m.

Neave, D. A. and K. D. Putirka (2017). "A New Clinopyroxene-Liquid Barometer, and Implications for Magma Storage Pressures under Icelandic Rift Zones". *American Mineralogist* 102.4, pp. 777–794. issn: 0003-004X. doi: 10/gdjcbj.

Oman, L., A. Robock, G. L. Stenchikov, and T. Thordarson (2006). "High-Latitude Eruptions Cast Shadow over the African Monsoon and the Flow of the Nile". *Geophysical Research Letters* 33.18, p. L18711. doi: 10/bsd9sz.

Oppenheimer, C., A. Orchard, M. Stoffel, T. P. Newfield, S. Guillet, C. Corona, M. Sigl, N. D. Cosmo, and U. Büntgen (2018). "The Eldgjá Eruption: Timing, Long-Range Impacts and Influence on the Christianisation of Iceland". *Climatic Change*, pp. 1–13. doi: 10/gc5r9x.

Pálsson, H. and P. Edwards (1972). *The Book of Settlements: Landnámabók*. University of Manitoba Icelandic Series. University of Manitoba Press. isbn: 0-88755-698-1.

Parcheta, C., S. Fagents, D. A. Swanson, B. F. Houghton, and T. Ericksen (2015). "Hawaiian Fissure Fountains: Quantifying Vent and Shallow Conduit Geometry, Episode 1 of the 1969–1974 Mauna Ulu Eruption". *Hawaiian Volcanoes: From Source to Surface*. Vol. 208. American Geophysical Union, pp. 369–391.

Pedersen, G. B. M. et al. (2017). "Lava Field Evolution and Emplacement Dynamics of the 2014–2015 Basaltic Fissure Eruption at Holuhraun, Iceland". *Journal of Volcanology and Geothermal Research* 340, pp. 155–169. doi: 10/gbnmtf.

Polacci, M., R. A. Corsaro, and D. Andronico (2006). "Coupled Textural and Compositional Characterization of Basaltic Scoria: Insights into the Transition from Strombolian to Fire Fountain Activity at Mount Etna, Italy". *Geology* 34.3, pp. 201–204. doi: 10/bxs48v.

Reynolds, H. I., M. T. Gudmundsson, T. Högnadóttir, E. Magnússon, and F. Pálsson (2017). "Subglacial Volcanic Activity above a Lateral Dyke Path during the 2014–2015 Bárdarbunga-Holuhraun Rifting Episode, Iceland". *Bulletin of Volcanology* 79.6, p. 38. doi: 10/gbkvj3.

Sable, J. E., B. F. Houghton, P. Del Carlo, and M. Coltelli (2006). "Changing Conditions of Magma Ascent and Fragmentation during the Etna 122 BC Basaltic Plinian Eruption: Evidence from Clast Microtextures". *Journal of Volcanology and Geothermal Research* 158.3–4, pp. 333–354. doi: 10/dk5rkn.

Sable, J. E., B. F. Houghton, C. J. N. Wilson, and R. J. Carey (2009). "Eruption Mechanisms during the Climax of the Tarawera 1886 Basaltic Plinian Eruption Inferred from Microtextural Characteristics of the Deposits". *Studies in volcanology. The legacy of George Walker. Geological Society, London*, pp. 129–154. doi: 10/gfs7jg.

Sahagian, D. L. and A. A. Proussevitch (1998). "3D Particle Size Distributions from 2D Observations: Stereology for Natural Applications". *Journal of Volcanology and Geothermal Research* 84.3–4, pp. 173–196. doi: 10/fwnv97.

Schmid, M. M. E., A. J. Dugmore, O. Vésteinsson, and A. J. Newton (2016). "Tephra Isochrons and Chronologies of Colonisation". *Quaternary Geochronology*. issn: 1871-1014. doi: 10/gbmvdp.

Schneider, C. A., W. S. Rasband, and K. W. Eliceiri (2012). "NIH Image to ImageJ: 25 Years of Image Analysis". *Nature Methods* 9.7, pp. 671–675. doi: 10/gcwb4q.

Shea, T., B. F. Houghton, L. Gurioli, K. V. Cashman, J. E. Hammer, and B. J. Hobden (2010). "Textural Studies of Vesicles in Volcanic Rocks: An Integrated Methodology". *Journal of Volcanology and Geothermal Research* 190.3-4, pp. 271–289. doi: 10/bmn9xt.

Sigl, M. et al. (2015). "Timing and Climate Forcing of Volcanic Eruptions for the Past 2,500 Years". *Nature* 523.7562, pp. 543–549. doi: 10/f3mxdb.

Sigurðardóttir, S. S., M. T. Gudmundsson, and S. Hreinsdóttir (2015). "Mapping of the Eldgjá Lava

Flow on Mýrdalssandur with Magnetic Surveying". *Jökull* 65, pp. 61–71.
Sparks, R. S. J. (2003). "Dynamics of Magma Degassing". *Geological Society, London, Special Publications* 213.1, pp. 5–22. DOI: 10/fsp8w9.
Stevenson, J. A., S. C. Loughlin, A. Font, G. W. Fuller, A. MacLeod, I. W. Oliver, B. Jackson, C. J. Horwell, T. Thordarson, and I. Dawson (2013). "UK Monitoring and Deposition of Tephra from the May 2011 Eruption of Grímsvötn, Iceland". *Journal of Applied Volcanology* 2.1, pp. 1–17. DOI: 10/gdh7xf.
Stovall, W. K., B. F. Houghton, H. Gonnermann, S. A. Fagents, and D. A. Swanson (2011). "Eruption Dynamics of Hawaiian-Style Fountains: The Case Study of Episode 1 of the Kīlauea Iki 1959 Eruption". *Bulletin of Volcanology* 73.5, pp. 511–529. DOI: 10/fk3ffk.
Stovall, W. K., B. F. Houghton, J. E. Hammer, S. A. Fagents, and D. A. Swanson (2012). "Vesiculation of High Fountaining Hawaiian Eruptions: Episodes 15 and 16 of 1959 Kīlauea Iki". *Bulletin of Volcanology* 74.2, pp. 441–455. DOI: 10/br2h7c.
Swanson, D. A. (1973). "Pahoehoe Flows from the 1969–1971 Mauna Ulu Eruption, Kilauea Volcano, Hawaii". *GSA Bulletin* 84.2, pp. 615–626. ISSN: 0016-7606. DOI: 10/c83frd.
Thordarson, T. (2003). "The 1783–1785 AD Laki-Grímsvötn Eruptions I: A Critical Look at the Contemporary Chronicles". *Jökull* 53, pp. 1–10.
Thordarson, T., G. Larsen, S. Steinthorsson, and S. Self (2003). "The 1783-1785 AD Laki-Grimsvotn Eruptions II: Appraisal Based on Contemporary Accounts". *Jökull* 53, pp. 11–48.
Thordarson, T., D. J. Miller, G. Larsen, S. Self, and H. Sigurdsson (2001). "New Estimates of Sulfur Degassing and Atmospheric Mass-Loading by the 934 AD Eldgjá Eruption, Iceland". *Journal of Volcanology and Geothermal Research* 108.1–4, pp. 33–54. DOI: 10/ft5wvg.
Thordarson, T. and S. Self (1993). "The Laki (Skaftár Fires) and Grímsvötn Eruptions in 1783–1785". *Bulletin of Volcanology* 55.4, pp. 233–263. DOI: 10/cj4wgx.
– (2003). "Atmospheric and Environmental Effects of the 1783–1784 Laki Eruption: A Review and Reassessment". *Journal of Geophysical Research* 108.D1. DOI: 10/cdtrgc.
Thordarson, T., S. Self, N. Oskarsson, and T. Hulsebosch (1996). "Sulfur, Chlorine, and Fluorine Degassing and Atmospheric Loading by the 1783–1784 AD Laki (Skaftár Fires) Eruption in Iceland". *Bulletin of Volcanology* 58.2-3, pp. 205–225. DOI: 10/drt354.
Walker, G. P. L. and R. Croasdale (1971). "Characteristics of Some Basaltic Pyroclastics". *Bulletin volcanologique* 35.2, pp. 303–317. DOI: 10/dxbxw6.
Waters, L. E. and R. A. Lange (2015). "An Updated Calibration of the Plagioclase-Liquid Hygrometer-Thermometer Applicable to Basalts through Rhyolites". *American Mineralogist* 100.10, pp. 2172–2184. ISSN: 0003-004X. DOI: 10/f7tw38.
Wilson, T. M., C. Stewart, V. Sword-Daniels, G. S. Leonard, D. M. Johnston, J. W. Cole, J. Wardman, G. Wilson, and S. T. Barnard (2012). "Volcanic Ash Impacts on Critical Infrastructure". *Physics and Chemistry of the Earth, Parts A/B/C*. Volcanic Ash: An Agent in Earth Systems 45–46, pp. 5–23. DOI: 10/fgwcv3.
Witt, T., T. R. Walter, D. Müller, M. T. Guðmundsson, and A. Schöpa (2018). "The Relationship Between Lava Fountaining and Vent Morphology for the 2014–2015 Holuhraun Eruption, Iceland, Analyzed by Video Monitoring and Topographic Mapping". *Frontiers in Earth Science* 6. ISSN: 2296-6463. DOI: 10/c84c.
Wohletz, K. H., B. Zimanowski, and R. Büttner (2013). "Magma-Water Interactions". *Modelling Volcanic Processes: The Physics and Mathematics of Volcanism*. Ed. by S. A. Fagents, T. K. P. Gregg, and R. M. C. Lopes. 1st. Cambridge: Cambridge University Press, p. 421. ISBN: 978-0-521-89543-9.
Wohletz, K. H. (1983). "Mechanisms of Hydrovolcanic Pyroclast Formation: Grain-Size, Scanning Electron Microscopy, and Experimental Studies". *Explosive Volcanism* 17.1–4, pp. 31–63. DOI: 10/bkxwwg.
– (1986). "Explosive Magma-Water Interactions: Thermodynamics, Explosion Mechanisms, and Field Studies". *Bulletin of Volcanology* 48.5, pp. 245–264. DOI: 10/dtpfsd.
Wylie, J. J., K. R. Helfrich, B. Dade, J. R. Lister, and J. F. Salzig (1999). "Flow Localization in Fissure Eruptions". *Bulletin of Volcanology* 60.6, pp. 432–440. DOI: 10/c6nfn3.
Zielinski, G. A., P. A. Mayewski, L. D. Meeker, S. Whitlow, M. S. Twickler, M. Morrison, D. A. Meese, A. J. Gow, and R. B. Alley (1994). "Record of Volcanism Since 7000 B.C. from the GISP2 Greenland Ice Core and Implications for the Volcano-Climate System". *Science* 264.5161, pp. 948–952. DOI: 10/cxhvgn.
Zielinski, G. A., M. S. Germani, G. Larsen, M. G. L. Baillie, S. Whitlow, M. S. Twickler, and K. Taylor (1995). "Evidence of the Eldgjá (Iceland) Eruption in the GISP2 Greenland Ice Core: Relationship to Eruption Processes and Climatic Conditions in the Tenth Century". *The Holocene* 5.2, pp. 129–140. DOI: 10/c9zhcb.
Zimanowski, B., R. Büttner, and V. Lorenz (1997). "Premixing of Magma and Water in MFCI Experiments". *Bulletin of Volcanology* 58.6, pp. 491–495. DOI: 10/dnncnn.
Zimanowski, B., R. Büttner, P. Dellino, J. D. L. White, and K. H. Wohletz (2015). "Magma-Water Interaction and Phreatomagmatic Fragmentation". *The Encyclopedia of Volcanoes*. Ed. by H. Sigurdsson. 2nd. Amsterdam: Academic Press, pp. 473–484.